CELLULAR NEUROSCIENCE

A hierarchy of PDZ domain scaffolding proteins clusters the Kv1 K^+ channel protein complex at the axon initial segment

Wei Zhang†, Victoria L. Palfini†, Yu Wu, Xiaoyun Ding, Allison J. Melton, Yudong Gao, Yuki Ogawa, Matthew N. Rasband*

Action potentials are initiated and modulated at the axon initial segment (AIS) by highly clustered ion channels. Voltage-gated Kv1 potassium channels underlie most outward AIS K^+ current. AIS Kv1 channels exist in a large protein complex including ADAM22, Caspr2, and LGI1. However, their clustering mechanisms remain unknown. Because Kv1 channels have a highly conserved PDZ-binding motif, we used CRISPR-based genome editing to screen 18 PDZ domain-containing proteins identified in our previous AIS proximity proteome for their AIS localization. Among these, we found that the scaffolding proteins SCRIB and PSD93 are highly enriched at the AIS. Using CRISPR-mediated knockout, cell surface clustering assays, and coimmunoprecipitation, we show that SCRIB and PSD93 bind to and are required for AIS Kv1 channel clustering, whereas SCRIB links the AIS Kv1 channel protein complex to the master AIS scaffolding protein AnkyrinG. These results define a hierarchy of scaffolding proteins that combine to cluster AIS Kv1 channels.

INTRODUCTION

The axon initial segment (AIS) generates and shapes axonal action potentials due to its high densities of voltage-gated sodium (Nav) and potassium (Kv) channels (*1*). Among the latter, AIS Kv1 channels (*2*) modulate action potential waveform and account for most of the outward AIS K^+ current in some neuronal cell types (*3*). AIS Kv1 channels are heterotetramers consisting of the pore-forming α subunits Kv1.1, Kv1.2, and Kv1.4 and accessory β subunits including Kvβ2 (*4*, *5*). Mutations in Kv1 channel α subunits cause seizures and epilepsy, highlighting their critical role as regulators of neuronal excitability (*6*). Despite their functional importance, the mechanisms responsible for the clustering of these Kv1 channels at the AIS are not understood.

Nav1, Kv7, and K2P leak K^+ channels are recruited to the AIS through direct binding to the master AIS scaffolding protein AnkyrinG (AnkG) (*7*–*11*). Although loss of AnkG in cultured neurons abolishes AIS Kv1 channel clustering (*12*), Kv1 channels lack the AnkG-binding motifs found in Nav1, Kv7, and K2P channels. Thus, the link between Kv1 channels and AnkG is unknown. Instead, Kv1 channel α subunits have C-terminal PDZ-binding motifs that interact with PDZ domain-containing proteins such as the membrane-associated guanylate kinase (MAGUK) family of scaffolding proteins (*13*, *14*). Surface clustering assays in heterologous cells and coimmunoprecipitation (co-IP) studies from brain homogenates demonstrate that Kv1 channels interact with PSD93 (encoded by the *Dlg2* gene), a MAGUK that is enriched at the AIS (*15*, *16*). We previously showed that silencing PSD93 expression in cultured neurons reduces Kv1 channel clustering at the AIS (*16*), but later studies using $Dlg2^{-/-}$ mice show preserved AIS Kv1 channel clustering in the brain and spinal cord (*15*, *17*). Thus, interactions with PSD93 alone cannot explain AIS Kv1 channel clustering, and PSD93 is unlikely to function as the link between Kv1 channels and AnkG.

Department of Neuroscience, Baylor College of Medicine, Houston, TX 77030, USA.
*Corresponding author. Email: rasband@bcm.edu
†These authors contributed equally to this work.

AIS Kv1 channels exist in a multiprotein complex that includes PSD93, the cell adhesion molecules (CAMs) Caspr2 (*Cntnap2*) and TAG1 (*Cntn2*) (*16*), the transmembrane protein ADAM22 (*Adam22*) (*15*), and LGI1 (*Lgi1*), a secreted binding partner of ADAM22 (*18*, *19*). However, none of these is required for AIS Kv1 channel clustering because $Cntnap2^{-/-}$, $Cntn2^{-/-}$, and $Adam22^{-/-}$ mice have intact AIS Kv1 channel clustering (*15*, *17*), although others report reduced AIS Kv1 channel clustering in $LgI1^{-/-}$ mice (*18*). Thus, other molecules and mechanisms must recruit and retain Kv1 channels at the AIS.

We recently used unbiased immunoproximity biotinylation to define the AIS proteome (*20*). Here, we used CRISPR-mediated genome editing to tag all 18 PDZ domain-containing proteins identified in our proteomic dataset; among these, we found that only PSD93 and SCRIB were enriched at the AIS. We used CRISPR-mediated disruption of *Scrib* and *Dlg2*, co-IPs, and surface clustering assays to demonstrate that SCRIB interacts with and clusters AIS Kv1 channels, PSD93, and ADAM22. We show that Kv1 channels interact with SCRIB in a PDZ-binding motif–dependent manner and that SCRIB links Kv1 channels and PSD93 to AnkG. Our results reveal that the mechanism of localization for AIS Kv1 channels is distinct from all other AIS ion channels. Instead of Kv1 channels binding to AnkG, the latter recruits the scaffolding protein SCRIB, while SCRIB and PSD93 cluster Kv1 channels.

RESULTS

PDZ domain-containing proteins enriched at the AIS

Each heterotetrameric Kv1 channel has four conserved C-terminal PDZ-binding motifs (*13*, *16*). Our previous work showed that the PDZ domain-containing protein PSD93 is found at the AIS and can cluster Kv1 channels in vitro (*16*). However, the mechanism linking AIS Kv1 channels to AnkG remains unknown, and loss of PSD93 in vivo does not disrupt AIS Kv1 channel clustering (*15*). Therefore, we considered whether other PDZ domain-containing proteins might also contribute to AIS Kv1 channel clustering. Using UniProt, we identified 144 nonredundant genes in rat that encode for PDZ domain-

containing proteins (data S1). We compared these against our recently reported immunoproximity labeling AIS (IPL-AIS) proteome (*20*). This comparison revealed that 18 PDZ domain-containing proteins are found in the IPL-AIS proteome (Fig. 1A). These were classified into four categories based on their number of PDZ domains (Fig. 1B).

To determine whether PDZ domain-containing proteins are enriched at the AIS, we used CRISPR-Cas9–mediated genome editing to tag each of the 18 candidates at their C termini with a spaghetti monster fluorescent protein with V5 epitope tags (smFP-V5) (*20*–*22*). Gene-specific guide RNAs (GS-gRNAs) were designed for smFP-V5 addition in the last exon, and knock-in plasmids were constructed and packaged in adeno-associated viral vectors (AAVs) (Fig. 1C). Beginning at day in vitro 1 (DIV1) and DIV2, neurons were transduced with two AAVs: one for Cas9 expression and one for the GS-gRNA and smFP-V5 for insertion by homology-independent repair. Transduced neurons were fixed 2 weeks later and immunolabeled using antibodies against βIV spectrin to label the AIS and V5 to label the endogenously tagged proteins. Among the 18 candidates we tested, we found that gRNAs targeting *Scrib* and *Dlg2* resulted in a strong V5 tag signal at the AIS (Fig. 1D; these genes encode SCRIB and PSD93, respectively). This result is consistent with our previous two reports of SCRIB and PSD93 at the AIS (*16*, *20*). Twelve other candidates showed only weak V5 signal at the AIS but stronger labeling in the somatodendritic region of the neuron (Fig. 1D). The remaining four candidates *Deptor*, *Ahnak*, *Magi3*, and *Pdzd2* are not included because we found that fewer than five positive knock-in neurons from three independent experiments and none showed AIS enrichment.

To determine the relative AIS enrichment of the successfully tagged PDZ domain-containing proteins, we quantified their polarity index using the ratio of the mean V5 signal in the AIS to that in proximal dendrites (Fig. 1E). This analysis showed a polarity index greater than 1 (=AIS enrichment) for both SCRIB and PSD93, but other candidates had a ratio at or less than 1. Immunolabeling of cultured hippocampal neurons using antibodies against SCRIB and PSD93 showed that both colocalize with AnkG at the AIS (Fig. 1F). Furthermore, line scans along the proximal axon showed AIS enrichment and similar fluorescence profiles for AnkG, SCRIB, and PSD93 (Fig. 1G). Together, these results strongly support the conclusion that the PDZ domain-containing scaffolds SCRIB and PSD93 are enriched at the AIS.

SCRIB is found at the AIS throughout the brain

We previously showed PSD93 at the AIS in the brain (*16*). To determine whether SCRIB is widely expressed at the AIS throughout the brain, and to determine when SCRIB is first detected in the brain, we immunostained coronal brain sections collected from postnatal day 1 (P1) and P4, and adult mice using antibodies against SCRIB and AnkG. Robust SCRIB labeling was observed at the AIS of neocortical neurons as early as P1 and persisted through adulthood (Fig. 2, A to C). Similarly, AIS SCRIB was found throughout the brain and in both neonatal and adult hippocampus and the piriform cortex (Fig. 2, A to C). We found that nearly all neurons in the neocortex, piriform cortex, and hippocampus with an AIS had SCRIB clustered at the AIS (Fig. 2D). Immunolabeling of GABAergic inhibitory neurons showed that 100% of parvalbumin (PV)–positive neurons also had strong SCRIB labeling at the AIS (Fig. 2, E and F). Together, these results show that SCRIB is highly enriched at the AIS of both excitatory and inhibitory neurons throughout the brain.

SCRIB is not found at nodes of Ranvier or juxtaparanodes

Nodes of Ranvier are thought to be evolutionary derivatives of the AIS because they have a similar molecular organization: Both have highly clustered AnkG, βIV spectrin, Neurofascin, Nav channels, Kv7 channels, and K2P leak K^+ channels (*10*, *23*, *24*). Juxtaparanodes flank nodes of Ranvier adjacent to the paranodal junctions, are located beneath the myelin sheath, and have high densities of a Kv1 channel protein complex that includes PSD93, ADAM22, LGI1, and the CAMs Caspr2 and TAG1 (*15*, *25*). However, these nodal and juxtaparanodal protein complexes do not overlap and are restricted to their distinct axonal domains in myelinated axons. The AIS also has the same Kv1 channel protein complex as the juxtaparanode (fig. S1). Thus, the AIS is a combination of the molecular organization of nodes and juxtaparanodes. On the basis of the similarity of the AIS to nodes and juxtaparanodes, we investigated whether SCRIB is clustered at nodes and juxtaparanodes. Unexpectedly, immunostaining of the corpus callosum, optic nerve, and sciatic nerve failed to detect any nodal or juxtaparanodal SCRIB (Fig. 3A) in the central nervous system or peripheral nervous system.

To further confirm that SCRIB is not clustered at nodes or juxtaparanodes, we used AAV and CRISPR-Cas9 to insert an smFP-V5 tag in SCRIB or βIV spectrin; we used βIV spectrin (*Sptbn4*) as a control because it is clustered at both the AIS and nodes of Ranvier (*26*). Three weeks after injection of AAV for expression of *Scrib*- or *Sptbn4*-specific gRNAs in adult Cas9 transgenic mice, we dissected retina and optic nerves and immunostained these for V5-tagged proteins. We detected V5-tagged βIV spectrin at the AIS in the retina and at nodes in the optic nerve (Fig. 3, C, D, F, and G). However, we only found V5-tagged SCRIB at the AIS in the retina and not at nodes or juxtaparanodes in the optic nerve (Fig. 3, E to G). Thus, although SCRIB is found at the AIS, it is not found at nodes or juxtaparanodes, suggesting unique regulatory mechanisms that may exclude SCRIB from these sites along myelinated axons.

SCRIB is required for AIS Kv1 channel clustering

AIS Kv1 channels consist of tetrameric complexes of Kv1.1, Kv1.2, and Kv1.4 α subunits (*2*, *16*). Immunolabeling and fluorescence intensity line scans of Kv1.1 and Kv1.2 show that SCRIB's AIS distribution overlaps with that for Kv1 channels (fig. S2, A to D). To determine the nanoscale distribution of SCRIB, we used stochastic optical reconstruction microscopy (STORM). Conventional immunofluorescence labeling showed colocalization between SCRIB and Nfasc at the AIS (Fig. 4A), whereas STORM imaging showed that SCRIB exists at the AIS in a highly periodic distribution (Fig. 4B). Using stimulated emission depletion (STED) microscopy, we visualized Kv1.1 and SCRIB as well as SCRIB and PSD93 simultaneously (Fig. 4C). We found that Kv1.1, SCRIB, and PSD93 colocalize and are all found in a highly periodic distribution with an average spacing of ~190 to 200 nm (Fig. 4D), like the spacing previously observed for AIS AnkG, actin, and βIV spectrin (*27*, *28*). To determine whether SCRIB is required for Kv1 channel clustering, we used CRISPR-Cas9–mediated knockout of SCRIB. We transduced DIV1 hippocampal neurons with Cas9 AAV together with AAV expressing control gRNAs or AAV expressing three *Scrib*-specific gRNAs (3XgRNAs); the neurons were subsequently fixed at DIV20. A hemagglutinin (HA) tag driven by the neuron-specific human synapsin 1 promoter in both control and *Scrib* gRNA AAVs was used to identify transduced neurons. We found that loss of SCRIB decreased Kv1.2 localization at the AIS but

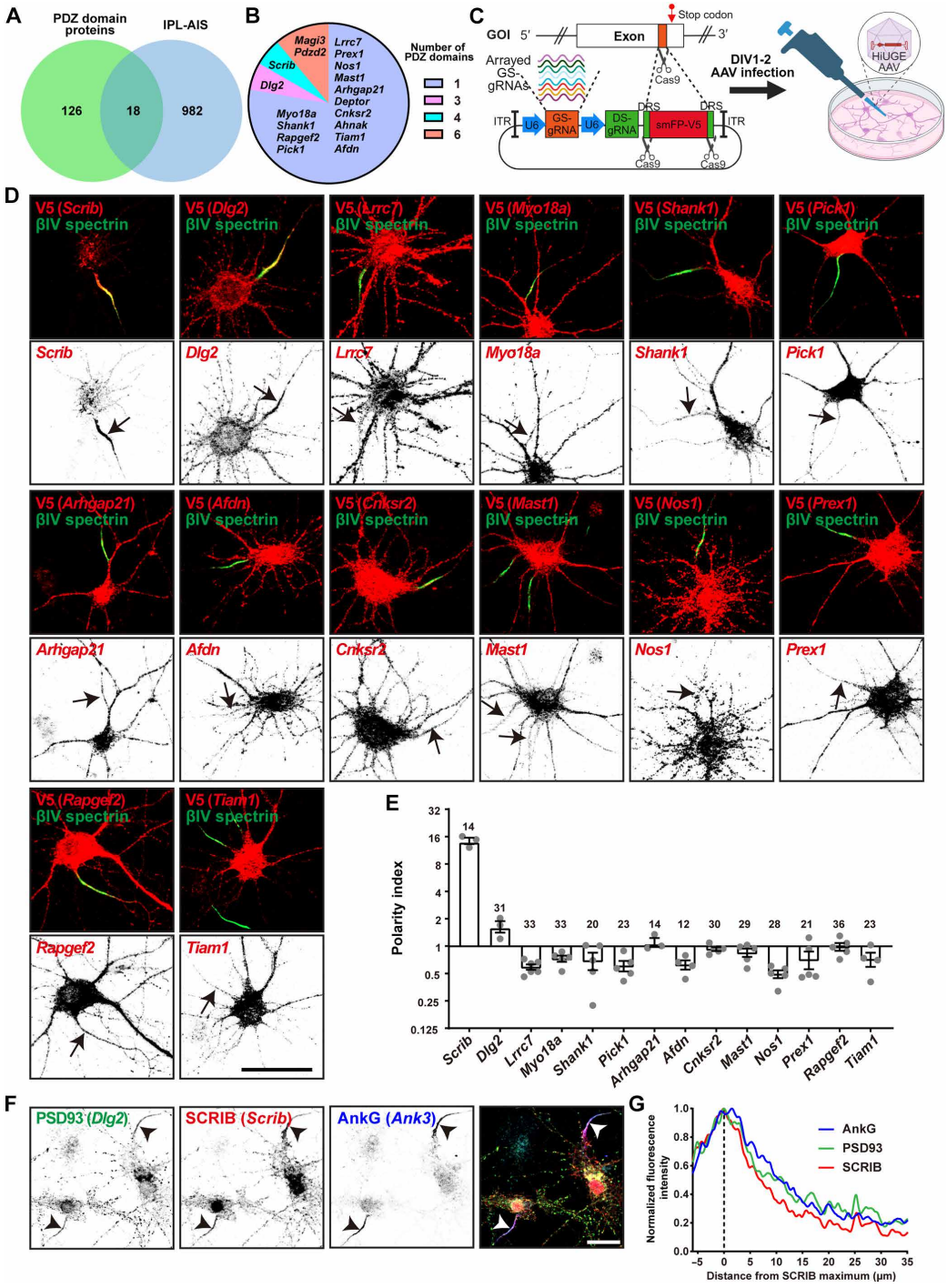

Fig. 1. SCRIB and PSD93 are PDZ domain-containing proteins at the AIS. (**A**) Venn diagram showing the overlap of PDZ domain-containing proteins in the rat genome and PDZ domain-containing proteins found in the top 1000 candidates from the IPL-AIS proteome. (**B**) Number of PDZ domains for the 18 PDZ domain-containing proteins tested here. (**C**) Cartoon illustrating the genome editing strategy. Plasmids harbor a DS-gRNA that recognizes DRSs flanking spaghetti monster fluorescent protein with V5 tags (smFP-V5) and a GS-gRNA targeting the last exon of the genes of interest allowing for insertion of smFP-V5 tags at the C terminus of each protein. Knock-in AAV plasmids were used for AAV production and neuronal transduction. Created in BioRender. M.N.R. (2025); https://BioRender.com/3q4w5px. (**D**) Representative images of smFP-V5 tagged proteins using GS-gRNAs against *Scrib*, *Dlg2*, *Lrrc7*, *Myo18a*, *Shank1*, *Pick1*, *Arhgap21*, *Afdn*, *Cnksr2*, *Mast1*, *Nos1*, *Prex1*, *Rapgef2*, and *Tiam1*. Cortical neurons were transduced at DIV2 with two AAVs, one for Cas9 expression and another for gene specific knock-in of smFP-V5. Cells were fixed at DIV16 and labeled for AIS using antibodies against βIV spectrin (green) and the V5 tag (red, targeted proteins). Arrows indicate the AIS of transduced neurons. Scale bar, 40 μm. (**E**) Quantification of V5 tag mean intensity in the AIS versus in the proximal dendrites. Three independent experiments were performed. The number of neurons counted is indicated. Data are means ± SEM. (**F**) Hippocampal neurons at DIV20 were stained with antibodies against PSD93 (green), SCRIB (red), and AnkG (blue). Arrowheads indicate the AIS. Scale bar, 20 μm. (**G**) Line scan of the average normalized AIS fluorescence intensity profile for AnkG (blue), PSD93 (green), and SCRIB (red). $n = 10$ neurons for each protein.

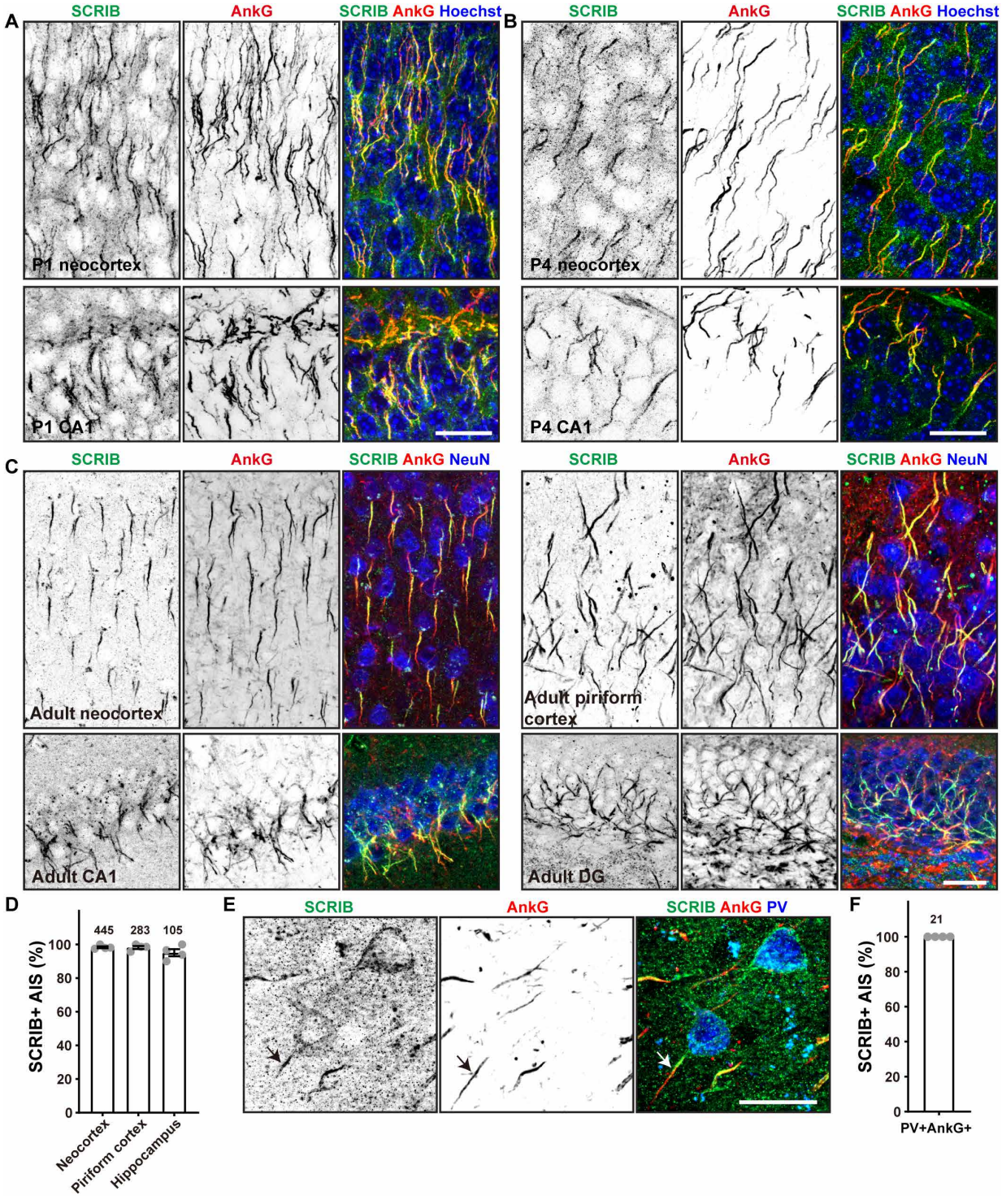

Fig. 2. SCRIB is enriched at the AIS throughout the brain. (**A** to **C**) Immunostaining of brain sections at P1 (A) and P4 (B) and in the adult brain (C). Samples were labeled with antibodies against SCRIB (green), AnkG (red, AIS), and Hoechst (blue, nuclei, A and B) or NeuN (blue, C). Layers II/III of the neocortex, pyramidal layers of the piriform cortex, CA1, and dentate gyrus (DG) of hippocampi are shown. Four independent experiments were performed. Scale bars, 20 μm. (**D**) Quantification of the percentage of SCRIB+ AIS in layers II/III of the neocortex, pyramidal layers of the piriform cortex, and CA1 regions of hippocampi. Four coronal tissue sections were quantified. The number of neurons examined is shown on the graph. Data are means ± SEM. (**E**) Immunostaining of PV+ inhibitory neurons. Adult coronal brain sections labeled for SCRIB (green), AnkG (red, AIS), and PV (blue). The arrow indicates the AIS of a PV+ neuron. Scale bar, 20 μm. (**F**) Quantification of the percentage of SCRIB+ AIS in PV+ neurons. Two independent experiments were performed with four coverslips analyzed ($n = 21$ PV+ neurons). Data are means ± SEM.

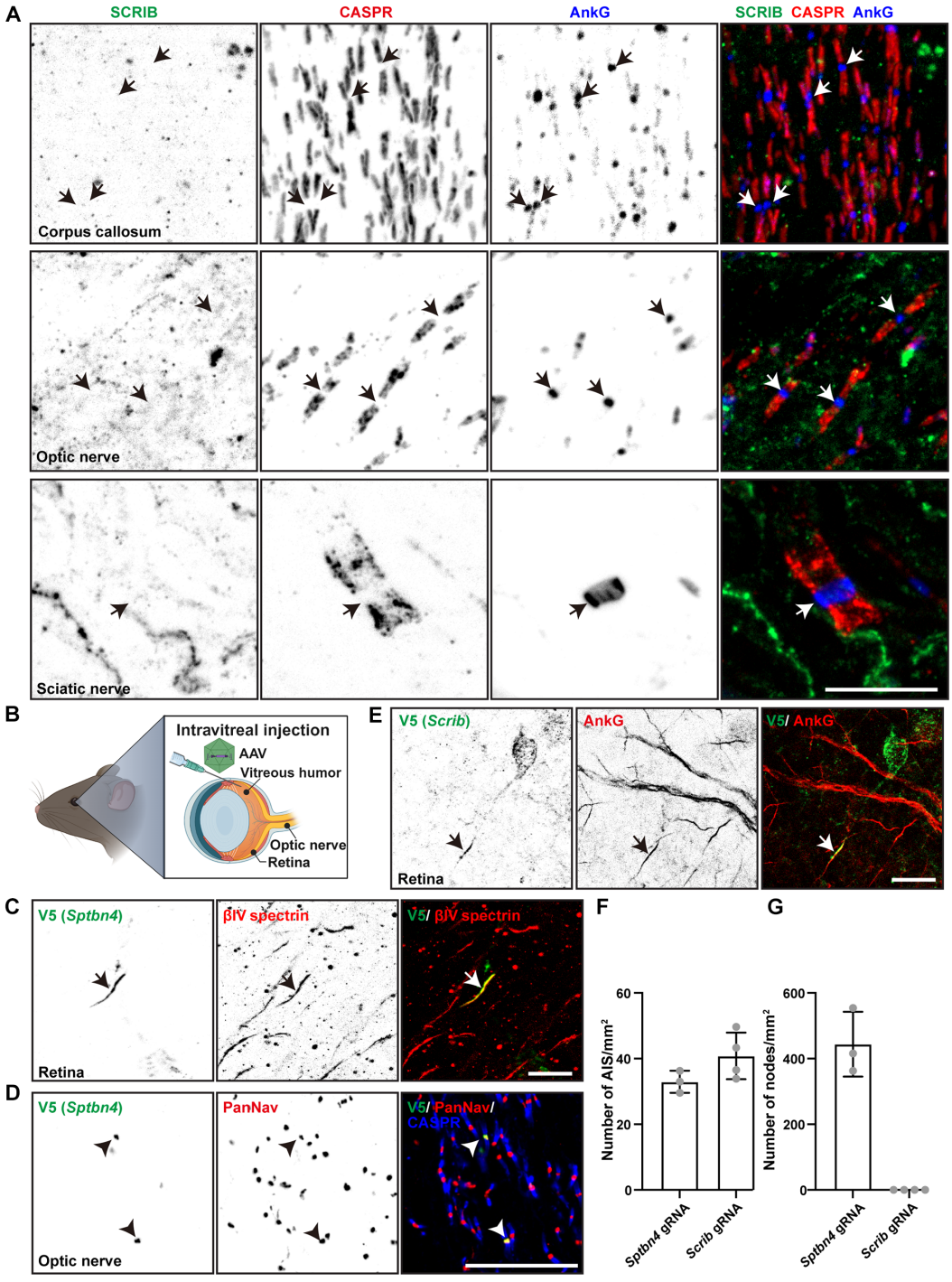

Fig. 3. SCRIB is excluded from nodes and juxtaparanodes. (**A**) Immunostaining of corpus callosum, optic nerve, and sciatic nerve in adult mice. Tissues were labeled for SCRIB (green), CASPR (red, paranodes), and AnkG (blue, nodes). Three independent experiments were performed. Arrows indicate nodes. Scale bar, 10 μm. (**B**) Cartoon illustrating the intravitreal injection of AAV in Cas9 knock-in mice. AAV was injected into the vitreous humor. Created in BioRender. M.N.R. (2025); https://BioRender.com/3q4w5px. (**C** and **D**) Immunolabeling of Cas9 knock-in mice that were intravitreally injected with *Sptbn4* knock-in AAV. Retinas and nerves were collected and immunostained 3 weeks later. AIS in transduced retinal ganglion cells (RGCs) were labeled using antibodies against V5 (green) and βIV spectrin (red) (C, arrows). Optic nerves were labeled using antibodies against V5 (green), Nav channels (PanNav, red), and CASPR (blue); arrowheads indicate nodes of Ranvier with V5-tagged βIV spectrin (D). Scale bars, 20 μm. (**E**) Immunolabeling of Cas9 knock-in mice that were intravitreally injected with *Scrib* knock-in AAV. Retinas and nerves were collected and immunostained 3 weeks later. V5 (green) and AnkG (red) labeling of the AIS in transduced RGCs (arrows). Scale bar, 20 μm. (**F**) Quantification of the number of AIS that show tagged βIV spectrin or SCRIB. Three to four mice were injected and used to count RGC AISs (22 to 24 microscope fields, 40x objective) analysis. Data are means ± SEM. (**G**) Quantification of the number of nodes that show tagged βIV spectrin or SCRIB. Three to four mice were injected and used to count nodes (23 to 24 microscope fields, 100x objective). Data are means ± SEM.

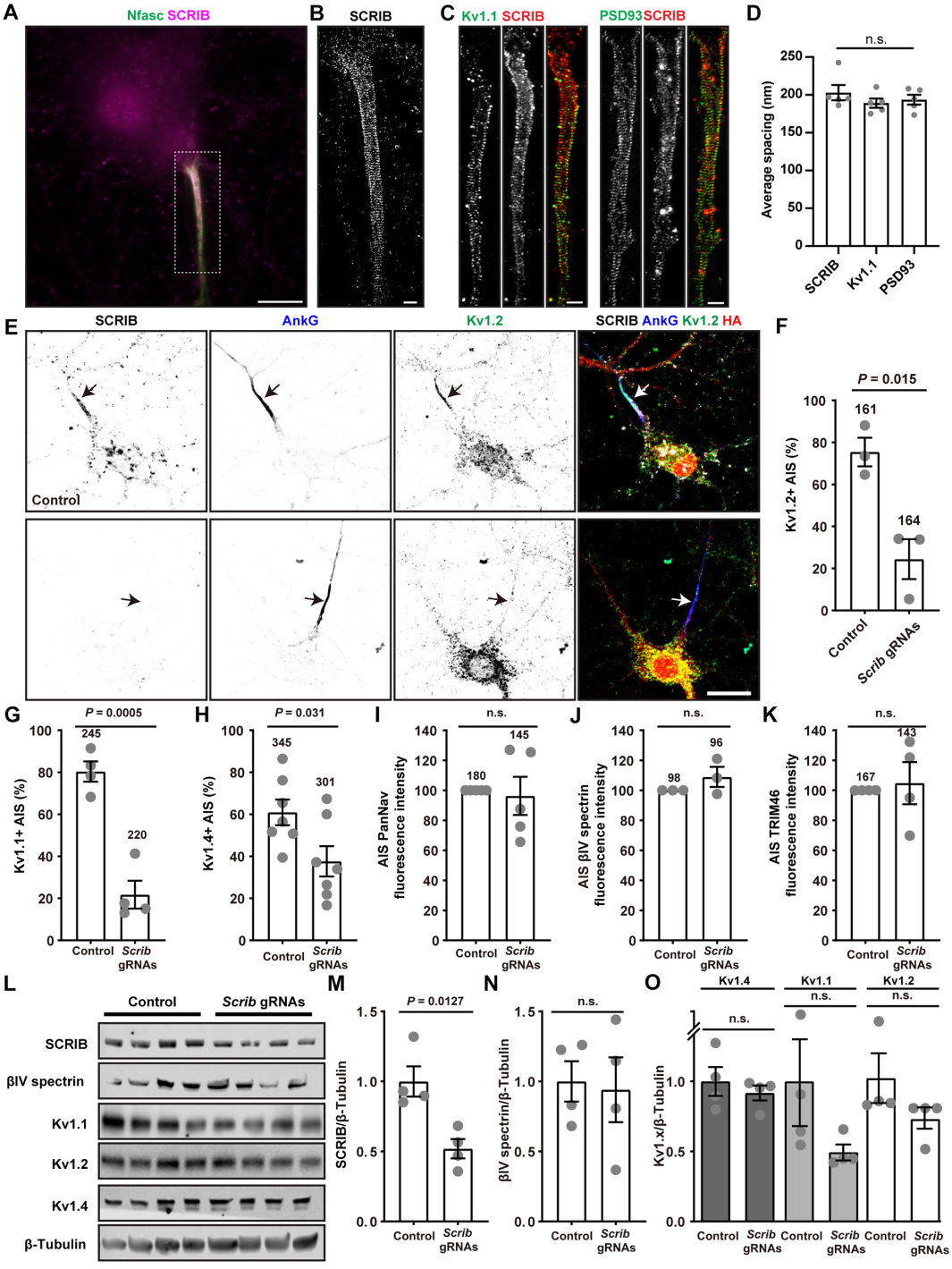

Fig. 4. SCRIB is necessary for AIS Kv1 channel clustering. (**A**) Immunostaining of DIV14 hippocampal neurons for SCRIB (magenta) and Nfasc (green). Nfasc is shown at 50% opacity. Scale bar, 10 μm. (**B**) STORM image of SCRIB from box in (A). Scale bar, 1 μm. (**C**) STED images of DIV22 hippocampal neurons immunostained for Kv1.1 or PSD93 (green) and SCRIB (red). Scale bar, 1 μm. (**D**) Spacing between the peak fluorescence for SCRIB, Kv1.1, and PSD93. $n = 5$ AIS per condition. Ordinary one-way ANOVA with Tukey's multiple comparisons test. n.s., not significant. Data are means ± SEM. (**E**) Immunostaining for SCRIB, AnkG, Kv1.2, and HA in DIV20 hippocampal neurons transduced at DIV0 with AAV to express Cas9 and control or *Scrib* 3XgRNAs; AAVs express HA. Arrows indicate the AIS. Scale bar, 20 μm. (**F** to **H**) Percentage of neurons with AIS Kv1.2 (F), Kv1.1 (G), and Kv1.4 (H) after transduction at DIV0 with control or *Scrib* 3XgRNAs and fixed at DIV20. $N = 3$ for Kv1.1 and Kv1.2, and $N = 7$ for Kv1.4. The number of neurons is shown. Data are means ± SEM. Unpaired two-tailed *t* test with Welch's correction. (**I** to **K**) AIS fluorescence intensity for Nav channels (I), βIV spectrin (J), and TRIM46 (K). Hippocampal neurons were transduced at DIV0 and fixed at DIV14 using control or *Scrib* 3XgRNAs. $N = 5$, 3, and 4 for PanNav, βIV spectrin, and TRIM46, respectively. The number of neurons is shown. Data are means ± SEM. Unpaired two-tailed *t* test with Welch's correction. (**L**) Immunoblots of cortical neurons transduced at DIV1 with Cas9 AAV and control or *Scrib* 3XgRNAs AAVs and lysed at DIV20. Blots were probed for SCRIB, βIV spectrin, Kv1.1, Kv1.2, Kv1.4, and β-Tubulin. (**M** to **O**) SCRIB, βIV spectrin, Kv1.1, Kv1.2, and Kv1.4 expression compared to β-Tubulin and normalized to controls. Data are means ± SEM. Unpaired two-tailed *t* test with Welch's correction.

did not affect the enrichment for AnkG (Fig. 4, E and F). Similarly, the percentage of Kv1.1- and Kv1.4-labeled AIS was also decreased after loss of SCRIB (Fig. 4, G and H). However, knockout of SCRIB did not affect other AIS proteins known to be clustered by AnkG including Nav channels, βIV spectrin, and TRIM46 (Fig. 4, I to K). Together, these results show that SCRIB is required for the clustering of Kv1 channels.

The loss of AIS Kv1 channels could be due to the loss of clustering, increased turnover and protein degradation, or reduced protein expression. To begin to distinguish among these possibilities, we performed immunoblotting of cultured neurons to determine the total amount of Kv1 channel subunits after knockout of SCRIB. As described above, we used CRISPR-Cas9 and *Scrib* 3XgRNAs to eliminate SCRIB. Although we observed a reduction in SCRIB protein, we did not find any change in the total amount of Kv1.1, Kv1.2, or Kv1.4 proteins or in the total amount of the AIS protein βIV spectrin (Fig. 4, L to O).

To further investigate the loss of AIS Kv1 channels and how this may affect neuronal excitability, we cultured mouse cortical neurons on multielectrode arrays (MEAs) and performed knockout of mouse *Scrib* using AAV to express control or *Scrib* 3XgRNAs in Cas9 transgenic neurons; we tested the efficacy of two separate gRNAs for their knockout efficiency (fig. S2, E and F). However, after loss of SCRIB, the overall network excitability was unaffected (fig. S2, G to J). This may reflect homeostatic changes in neuronal excitability and suggests that the reduction in AIS Kv1 channels by immunofluorescence reflects loss of Kv1 channel clustering due to loss of SCRIB rather than loss of total protein.

SCRIB interacts with Kv1 channels

To determine whether SCRIB, like PSD93, interacts directly with Kv1 channels, we performed a surface clustering assay in COS7 cells. In this assay, membrane proteins are recruited by PDZ domain-containing proteins into cell surface clusters, indicating an interaction between the membrane protein and PDZ domain-containing protein (*13*). When expressed individually, Kv1 channel α subunits, PSD93, and SCRIB are distributed throughout the cell and do not form surface clusters (Fig. 5A). However, upon coexpression of PSD93 with the Kv1 channel α subunits Kv1.1 and Kv1.4, Kv1 channels redistribute into large membrane surface clusters; these channels are on the cell surface because they are detected in unpermeabilized cells with an antibody that recognizes an extracellular epitope of Kv1.1 (Kv1.1ext) (Fig. 5B, top, arrowheads). Similarly, when SCRIB, Kv1.1, and Kv1.4 are coexpressed, large clusters containing all three proteins can be detected on the cell surface with the Kv1.1ext antibody (Fig. 5B, bottom, arrowheads). Together, these results show that Kv1 channel α subunits interact with SCRIB and PSD93. Kv1.4 and SCRIB also cocluster with ADAM22 (figs. S3, A, D, E, and F, arrowheads), a PDZ-binding motif–containing protein found at the AIS that also associates with Kv1 channels and PSD93 (fig. S3, B, C, and F) (*15*). ADAM22 also interacts with the extracellular protein LGI1 at the AIS (*18*). Together, these results show that SCRIB and PSD93 can form surface clusters with Kv1 channels and ADAM22.

To further show that SCRIB interacts with Kv1 channels, we performed co-IPs using human embryonic kidney (HEK) 293T cells transfected with plasmids to express Kv1.4 and FLAG-tagged SCRIB (SCRIB-FLAG). We used Kv1.4 because homotetrameric Kv1.4 channels are trafficked to the cell surface more efficiently than homotetrameric Kv1.1 and Kv1.2 channels, which tend to be retained in the endoplasmic reticulum (ER) (*4*, *29*) (see the Kv1.1 single transfection in Fig. 5A showing prominent ER-retained Kv1.1). We found that Kv1.4 coimmunoprecipitates with SCRIB-FLAG (Fig. 5C). We confirmed these results with the reciprocal IP using an anti-Kv1.4 antibody. We found that SCRIB-FLAG coimmunoprecipitates with Kv1.4 (Fig. 5D). Kv1.2 also coimmunoprecipitates with Kv1.4 and SCRIB-FLAG in HEK293T cells expressing Kv1.2/Kv1.4 heterotetramers and SCRIB-FLAG (fig. S3G). Together, these results show that SCRIB interacts with Kv1 channels.

To determine whether the PDZ-binding motif in Kv1 channels is necessary for SCRIB-dependent channel clustering, we generated a Kv1.4 mutant construct (Kv1.4ΔPDZ) lacking the last four amino acids (ETDV), which are essential for its interaction with PDZ domain-containing proteins (*13*). We included PSD93 as a positive control because the PDZ-binding motif of Kv1.4 was previously shown to be required for its interaction with PSD93 (*13*). When coexpressed, wild-type Kv1.4 and PSD93 colocalize in large clusters (Fig. 5E, arrowheads). In contrast, when Kv1.4ΔPDZ is cotransfected with PSD93, these proteins do not form clusters and instead are located throughout the cell (Fig. 5E), like the staining pattern of singly transfected Kv1.4ΔPDZ (Fig. 5A). Thus, the PDZ-binding motif of Kv1.4 is necessary for its ability to form clusters with PSD93 in COS cells. Like PSD93, coexpression of SCRIB with Kv1.4 causes the redistribution of these proteins into clusters (Fig. 5F, arrowheads). However, deletion of the Kv1.4 PDZ-binding motif (Kv1.4ΔPDZ) blocks the ability of SCRIB to interact and form clusters (Fig. 5F), and both SCRIB and Kv1.4ΔPDZ are distributed diffusely throughout the cells. Quantification of the percent of transfected cells with large clusters reveals that the deletion of Kv1.4's PDZ-binding motif notably reduces the clustering of the PDZ proteins PSD93 and SCRIB with Kv1.4 (Fig. 5G). Together, these results show that the interaction between SCRIB and Kv1.4 is PDZ-binding motif dependent.

SCRIB contributes to AIS PSD93 clustering

To determine whether AIS Kv1 channel clustering requires the scaffolds AnkG or PSD93, we used CRISPR-Cas9 and 3XgRNAs to delete AnkG and PSD93. Consistent with one prior report (*12*), we found that loss of AnkG blocked the clustering of AIS Kv1.1, Kv1.2, and βIV spectrin (fig. S4, A to D). Similarly, and consistent with our previous in vitro study (*16*), we found that knockout of PSD93 reduced the number of Kv1.1 and Kv1.2-labeled AIS but had no effect on AIS βIV spectrin (fig. S4, A, E to G).

To determine how SCRIB, AnkG, and PSD93 influence each other's AIS localization, we used CRISPR-Cas9 and 3XsgRNAs to delete these scaffolds one by one. We found that loss of SCRIB had no effect on AnkG but substantially reduced the AIS enrichment of PSD93 (Fig. 6A). Quantification of AIS AnkG after loss of SCRIB showed no difference in either the number of neurons with AnkG-labeled AIS or the AIS AnkG fluorescence intensity (Fig. 6B). In contrast, although most neurons still had some residual PSD93 labeling at the AIS (Fig. 6A), the AIS PSD93 fluorescence intensity was reduced (Fig. 6C). Consistent with its role as the master organizer of AIS assembly, knockout of AnkG blocked the clustering of both SCRIB and PSD93 at the AIS (Fig. 6, D to G). In contrast to SCRIB's regulation of PSD93, we found that, although 3XgRNAs targeting *Dlg2* completely eliminated PSD93 labeling at the AIS (Fig. 6, D and H), they had no effect on either SCRIB or AnkG (Fig. 6, D, I, and J). Together, these results suggest a hierarchy for these scaffolds where SCRIB clusters PSD93 and AnkG clusters SCRIB.

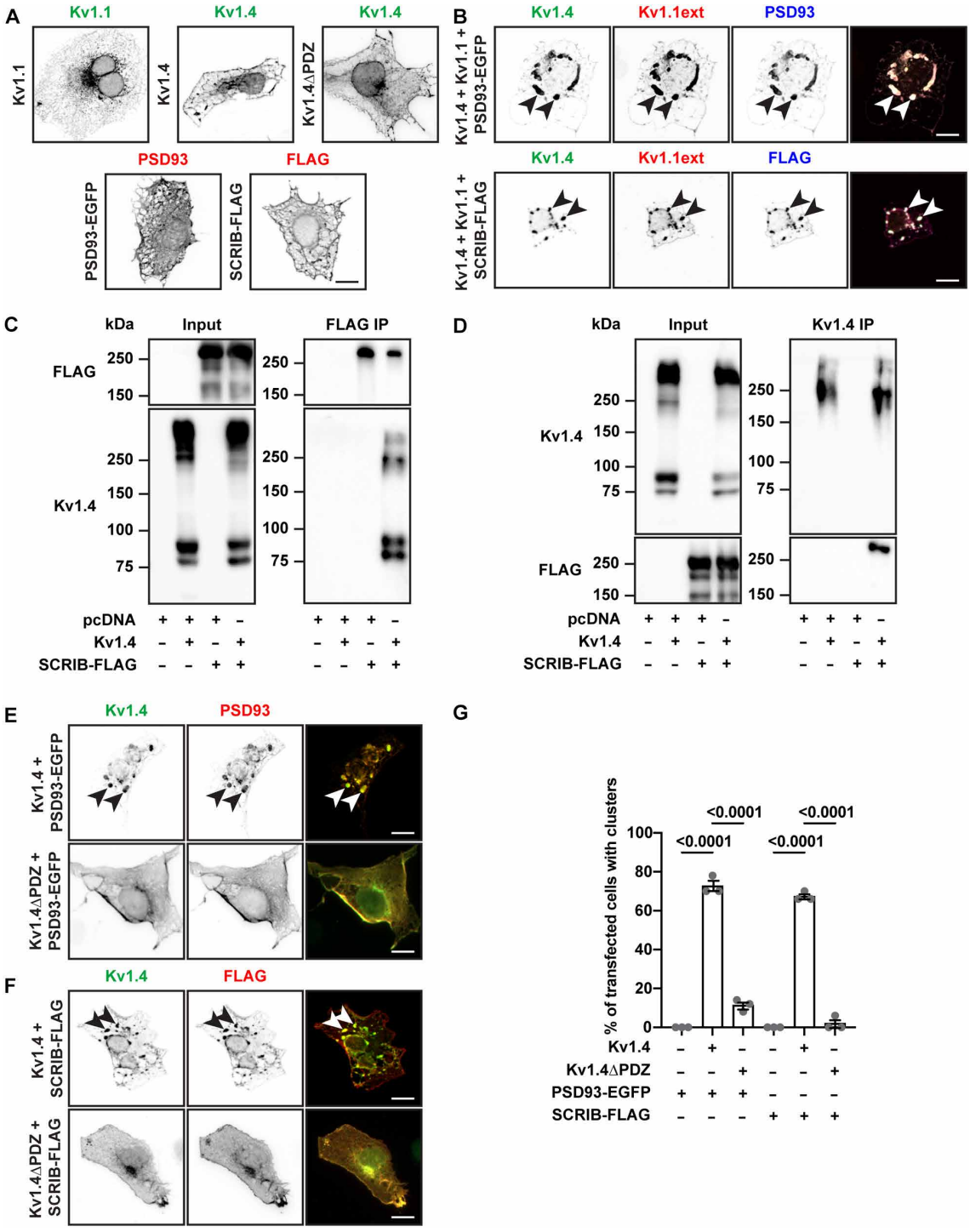

Fig. 5. SCRIB and PSD93 cluster Kv1 channels. (**A**) Representative images of COS7 cells expressing Kv1 channel α subunits, a Kv1.4 deletion mutant lacking the PDZ-binding motif (Kv1.4ΔPDZ), PSD93-EGFP, and SCRIB-FLAG. The DNA constructs used for the transfections are indicated to the left of each image, and the antibodies used for immunostaining are indicated above each image. Scale bar, 10 μm. (**B**) Cotransfection of Kv1.4, Kv1.1, and PSD93-EGFP or SCRIB-FLAG in COS7 cells. An antibody directed against the extracellular domain of Kv1.1 (Kv1.1ext) was used to detect surface Kv1.1 prior to fixing and permeabilizing the cells. Arrowheads indicate examples of coclustered proteins. Scale bars, 10 μm. (**C** and **D**) Co-IP of SCRIB-FLAG and Kv1.4 in HEK293T cells with anti-FLAG antibody (C) or anti-Kv.1.4 antibody (D). The DNA constructs used for the transfections are indicated below each image, and the antibodies used for immunoblotting are indicated to the left of image. Input, 10-μg protein per lane. IP, from 10-μg protein per lane (C) or 40-μg protein per lane (D). (**E** and **F**) Cotransfection of PSD93-EGFP (E) or SCRIB-FLAG (F) and Kv1.4 or Kv1.4ΔPDZ in COS7 cells. Arrowheads indicate examples of coclustered proteins. Scale bars, 10 μm. (**G**) Quantification of the percentage of transfected cells with large clusters. $N = 3$ independent experiments per transfection condition, with 50 transfected cells counted per experiment and transfection condition. Ordinary one-way ANOVA with Tukey's multiple comparisons test. Adjusted P values are shown on the graph. Data are means ± SEM.

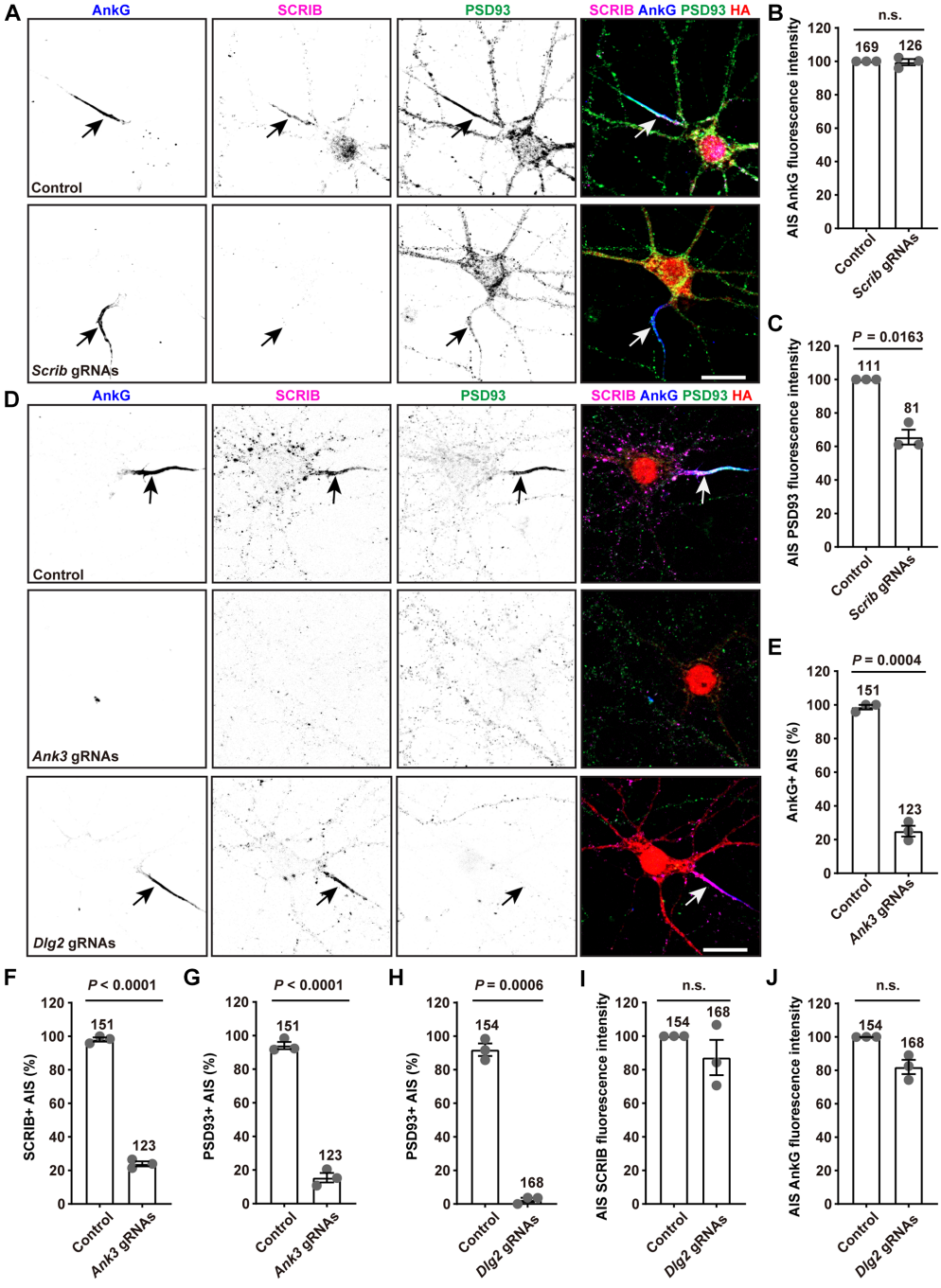

Fig. 6. AIS scaffolds regulate each other's AIS localization. (**A**) Hippocampal neurons immunostained for SCRIB (magenta), AnkG (blue), and PSD93 (green). Arrows indicate the AIS. Neurons were transduced at DIV0 with Cas9 AAV and with AAV to express control plasmids or *Scrib* 3XgRNAs; the control and 3XgRNA plasmids harbor an HA expression cassette. Neurons were fixed at DIV20. Scale bar, 20 μm. (**B** and **C**) Quantification of AIS AnkG (B) and PSD93 (C) fluorescence intensity in hippocampal neurons transduced with control or *Scrib* 3XgRNAs. $N = 3$ independent experiments. The number of neurons measured for each condition is shown. Data are means ± SEM. Unpaired two-tailed *t* test followed by Welch's correction. (**D**) Hippocampal neurons immunostained for SCRIB (magenta), AnkG (blue), and PSD93 (green). Arrows indicate the AIS. Neurons were transduced at DIV0 with Cas9 AAV and with AAV to express control plasmids, *Ank3* 3XgRNAs, or *Dlg2* 3XgRNAs. The control and 3XgRNA plasmids harbor an HA expression cassette. Neurons were fixed at DIV20. Scale bar, 20 μm. (**E** to **G**) Percentage of neurons with AnkG+ (E), SCRIB+ (F), or PSD93+ AIS (G) after transduction with control or *Ank3* 3XgRNAs. Neurons were transduced at DIV0 and fixed at DIV20. The number of neurons measured for each condition is shown. $N = 3$ independent experiments. Data are means ± SEM. Unpaired two-tailed *t* test followed by Welch's correction. (**H**) Percentage of hippocampal neurons with PSD93+ AIS after transduction with control or *Dlg2* 3XgRNAs. Neurons were transduced at DIV0 and fixed at DIV20. The number of neurons measured for each condition is shown on the graph. $N = 3$ for each experiment. Data are means ± SEM. Unpaired two-tailed *t* test followed by Welch's correction. (**I** and **J**) Quantification of AIS SCRIB (I) and AnkG (J) fluorescence intensity. $N = 3$ independent experiments. The number of neurons measured for each condition is shown. Data are means ± SEM. Unpaired two-tailed *t* test followed by Welch's correction.

SCRIB links the AIS Kv1 channel protein complex to AnkG

We showed the scaffolding proteins SCRIB, PSD93, and AnkG are required for AIS Kv1 channel localization in cultured hippocampal neurons (Fig. 4 and fig. S4). Furthermore, both SCRIB and PSD93 interact with Kv1 channels in a PDZ-binding motif–dependent manner, and like Kv1 channels, their AIS localization depends on AnkG (Fig. 6, E to G). These observations suggest that SCRIB may link Kv1 channels to AnkG. In *Drosophila*, SCRIB forms a complex with DLG, a MAGUK protein that has five mammalian homologs including PSD93 (*Dlg2*) (*30*, *31*). Thus, we speculate that PSD93 may also interact indirectly with AnkG through SCRIB. To test these possibilities, we first determined whether SCRIB and PSD93 interact. We expressed green fluorescent protein (GFP)–tagged PSD93 (PSD93-EGFP) and SCRIB-FLAG in HEK293T cells and performed co-IP experiments. We found that PSD93-EGFP coimmunoprecipitates with SCRIB-FLAG (Fig. 7A). Similarly, SCRIB-FLAG coimmunoprecipitates with PSD93-EGFP (Fig. 7B). Together, these results show that SCRIB and PSD93 interact.

To determine whether SCRIB can simultaneously interact with Kv1 channels and AnkG, we performed surface clustering assays by coexpressing Kv1.4, AnkG, and SCRIB or Kv1.4, AnkG, and PSD93 in COS7 cells. Coexpression of AnkG with Kv1.4 (Fig. 7C), AnkG with PSD93 (Fig. 7D), or AnkG with SCRIB (Fig. 7E) did not result in the formation of any clusters. The pattern of introduced protein localization resembled that of cells transfected only with AnkG (Fig. 7C). Although triple transfection of Kv1.4, PSD93, and AnkG resulted in the formation of Kv1.4 and PSD93-containing clusters, AnkG was not part of these clusters (Fig. 7F, arrowheads), suggesting that AnkG does not bind to PSD93. However, when Kv1.4, AnkG, and SCRIB were coexpressed, all three proteins colocalized in large clusters (Fig. 7G, arrowheads). We quantified the percentage of transfected cells with clustered AnkG and found clusters formed only in cells cotransfected with SCRIB, Kv1.4, and AnkG (Fig. 7H). Together, these results suggest that SCRIB links the AIS Kv1 channel protein complex, including PSD93, to AnkG.

SCRIB and PSD93 function synergistically

Single deletion of SCRIB or PSD93 reduces AIS Kv1.2 channel clustering by 60 to 80% (Figs. 4, F to H, and 8B, and fig. S4, E and F). However, deletion of SCRIB alone only reduces AIS PSD93 by 40% (Fig. 6C) and loss of PSD93 alone has no effect on AIS SCRIB (Fig. 6I). Thus, AIS SCRIB is not sufficient for the AIS clustering of Kv1 channels and likely functions synergistically with PSD93 to assemble and maintain the AIS Kv1 channel protein complex. To test this, we transduced neurons with both *Scrib* and *Dlg2* 3XgRNAs, and Cas9, to determine the effect of loss of both scaffolds on the clustering of AnkG and Kv1 channels (Fig. 8A). We found that, although AnkG was unaffected, loss of both SCRIB and PSD93 reduced the percentage of neurons with AIS Kv1 channels by more than 90% (Fig. 8B). Together, these results suggest that SCRIB and PSD93 function together to recruit and stabilize AIS Kv1 channels.

DISCUSSION

Here, we report a previously unknown molecular model that explains how the AIS Kv1 channel protein complex is enriched at the AIS (Fig. 8C). Using CRISPR-based genome editing, we evaluated PDZ domain-containing proteins to determine whether they are enriched at the AIS. Among these, we found that SCRIB and PSD93 are enriched at the AIS. These were further validated using antibodies. SCRIB and PSD93 interact with each other, with Kv1 channels through the channel's C-terminal PDZ-binding motifs, and they form surface clusters in COS7 cells when coexpressed with Kv1 channels. SCRIB is found at the AIS throughout the brain and in both excitatory and inhibitory neurons. SCRIB is also required for AIS enrichment of Kv1 channels and PSD93, whereas loss of PSD93 only affects Kv1 channels and not SCRIB clustering. However, loss of AnkG prevents AIS enrichment for both SCRIB and PSD93. Because AnkG, SCRIB, and Kv1 channels (but not AnkG, PSD93, and Kv1 channels) can form surface clusters, SCRIB is subordinate to AnkG in the hierarchy of AIS scaffolds, whereas PSD93 is subordinate to SCRIB. Thus, although both SCRIB and PSD93 can cluster Kv1 channels and both are necessary for proper AIS Kv1 channel clustering, only SCRIB can link Kv1 channels and PSD93 to AnkG, the master organizer of the AIS (Fig. 8C).

Mammalian SCRIB was previously reported to play key roles in neural tube closure, planar cell polarity, apical dendrite development, and at neuronal synapses (*32*, *33*). We show here that SCRIB also functions to cluster and link to AIS AnkG, a large Kv1 channel-containing protein complex that includes Kv1 channels, PSD93, ADAM22, Caspr2, TAG1, and LGI1. Both ADAM22 and Caspr2 have C-terminal PDZ-binding motifs, and we showed that ADAM22 can form surface clusters with both SCRIB (fig. S3) and PSD93 (*15*). Whether Caspr2 also interacts with these scaffolds through its PDZ-binding motif is unknown. Together, these observations highlight the central role SCRIB may play in regulating AIS properties and neuronal excitability through this larger Kv1 channel-containing protein complex. Consistent with this view, human pathogenic variants in *ADAM22 (*ADAM22), *CNTNAP2* (Caspr2), and *LGI1* (LGI1) all have phenotypic similarities including epilepsy and seizures (*34*–*37*).

Among the 18 PDZ domain-containing proteins identified in our AIS proximity proteome, only SCRIB and PSD93 were found at the AIS. These results are consistent with our previous reports showing SCRIB at the AIS by immunolabeling and tagging of SCRIB using genome editing (*20*) and PSD93 at the AIS by immunostaining (*16*). However, it is important to note that one limitation of the approach used here is that insertion of the epitope tag occurs by homology-independent repair in the last exon of each candidate protein, with the epitope tag replacing the coding sequence beyond where the repair occurs. It is possible the replacement of the C terminus of some PDZ domain-containing proteins with the smFP-V5 tag may disrupt their AIS enrichment. Thus, the absence of the epitope-tagged protein from the AIS does not exclude the candidate as an AIS enriched protein. Further examination of the remaining 16 candidates can be performed by N-terminal tagging and through immunolabeling with stringently validated antibodies.

Although our results strongly support a model where SCRIB links the Kv1 channel protein complex to AnkG, we were unable to test this in vivo. We successfully deleted SCRIB from some neurons in the brain using CRISPR-based approaches, but we were unable to reliably and reproducibly immunolabel AIS Kv1 channels due to the requirement for antigen retrieval or novel fixation methods. For reasons that are unclear, the dense cytoskeleton found at the AIS precludes robust immunostaining of the AIS Kv1 channel protein complex using conventional paraformaldehyde (PFA) fixation. Similarly, AIS K2P channels can only be detected at the AIS using a glyoxal-based fixative (*10*, *38*); however, glyoxal fixation did not improve AIS Kv1 channel labeling.

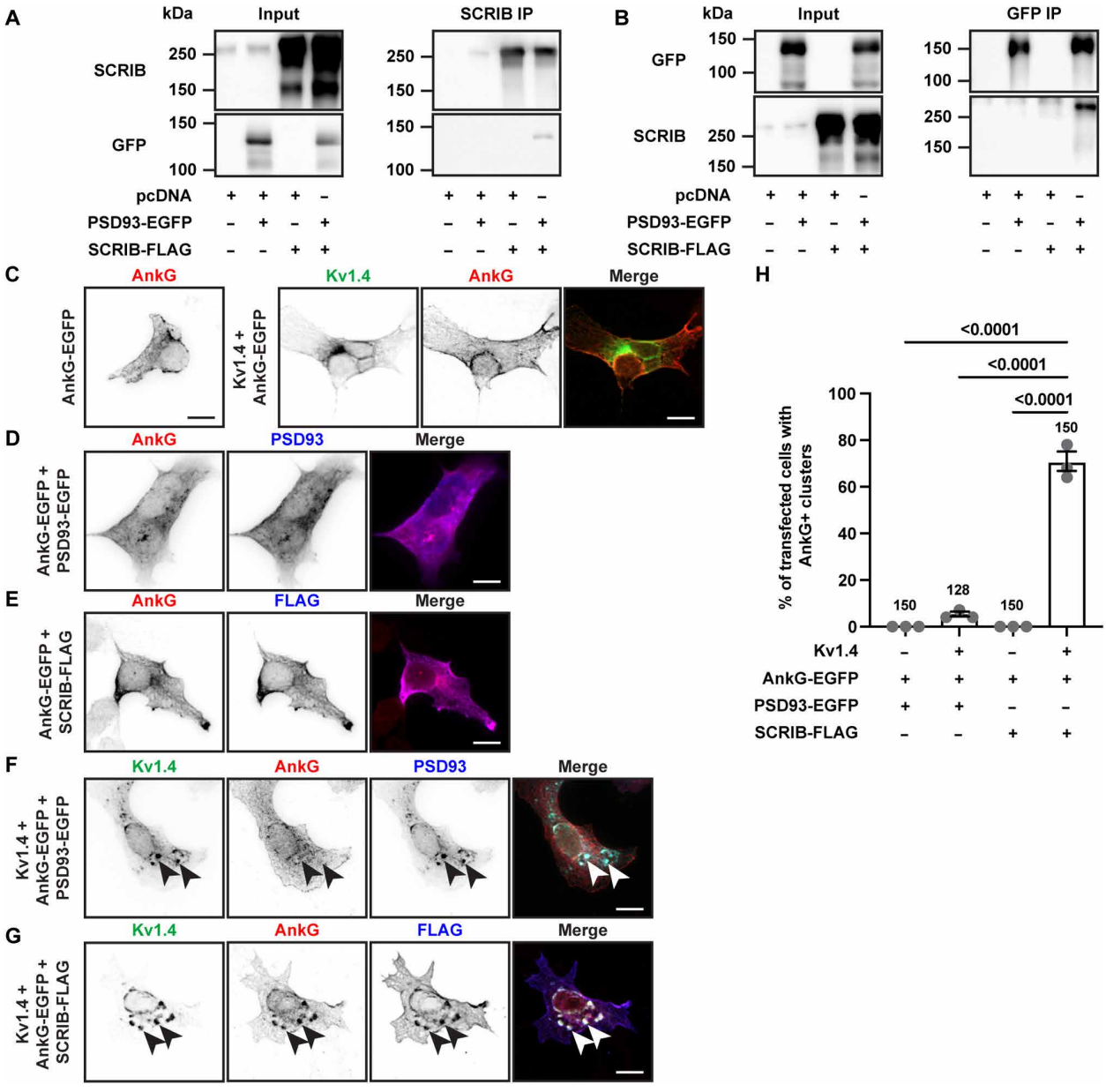

Fig. 7. AnkG can be recruited into Kv1 channel clusters by SCRIB. (**A** and **B**) Co-IP of SCRIB-FLAG and PSD93-EGFP in HEK293T cells with anti-SCRIB antibody (A) or anti-GFP antibody (B). Input, 10-μg protein per lane. IP, from 40-μg protein per lane. (**C**) Single transfection of AnkG-EGFP and cotransfection of Kv1.4 and AnkG-EGFP in COS7 cells. Scale bar, 10 μm. (**D**) Cotransfection of AnkG-EGFP and PSD93-EGFP in COS7 cells. Scale bar, 10 μm. (**E**) Cotransfection of AnkG-EGFP and SCRIB-FLAG in COS7 cells. Scale bar, 10 μm. (**F**) Cotransfection of Kv1.4, AnkG-EGFP, and PSD93-EGFP in COS7 cells. Arrowheads indicate examples of coclustered Kv1.4 and PSD93. Scale bar, 10 μm. (**G**) Cotransfection of Kv1.4, AnkG-EGFP, and SCRIB-FLAG. Arrowheads indicate examples of coclustered Kv1.4, AnkG, and SCRIB. Scale bar, 10 μm. (**H**) Quantification of the percentage of transfected cells with large AnkG+ clusters. $N = 3$ independent experiments per transfection condition. The number of cells counted is shown on the graph. Ordinary one-way ANOVA with Tukey's multiple comparisons test. Data are means ± SEM.

Intriguingly, a nearly identical Kv1 channel protein complex also exists in myelinated axons at the juxtaparanodes flanking nodes of Ranvier; these can be detected using conventional PFA fixation. Instead of SCRIB and PSD93, juxtaparanodes have PSD95 and PSD93, but simultaneous deletion of both MAGUK scaffolds has no effect on juxtaparanodal Kv1 channel clustering (*25*, *39*); PSD95 is not found at the AIS. Juxtaparanodes also have ADAM23, LGI2, and LGI3, and the juxtaparanodal clustering of Kv1 channels depends on these membrane and extracellular proteins (*40*). In our hands, we observed both LGI2 and LGI3 at the AIS but not ADAM23. Thus, at juxtaparanodes, extracellular interactions through ADAM23 and LGI proteins regulate Kv1 channel clustering, whereas cytoplasmic interactions through SCRIB regulate AIS Kv1 channel clustering. Despite SCRIB's ability to bind AnkG, it is not found at nodes of Ranvier; SCRIB is excluded from both nodes and juxtaparanodes despite SCRIB-binding proteins being present in both domains. These observations suggest mechanisms that actively exclude SCRIB from myelinated axons or that SCRIB simply cannot be trafficked beyond the AIS.

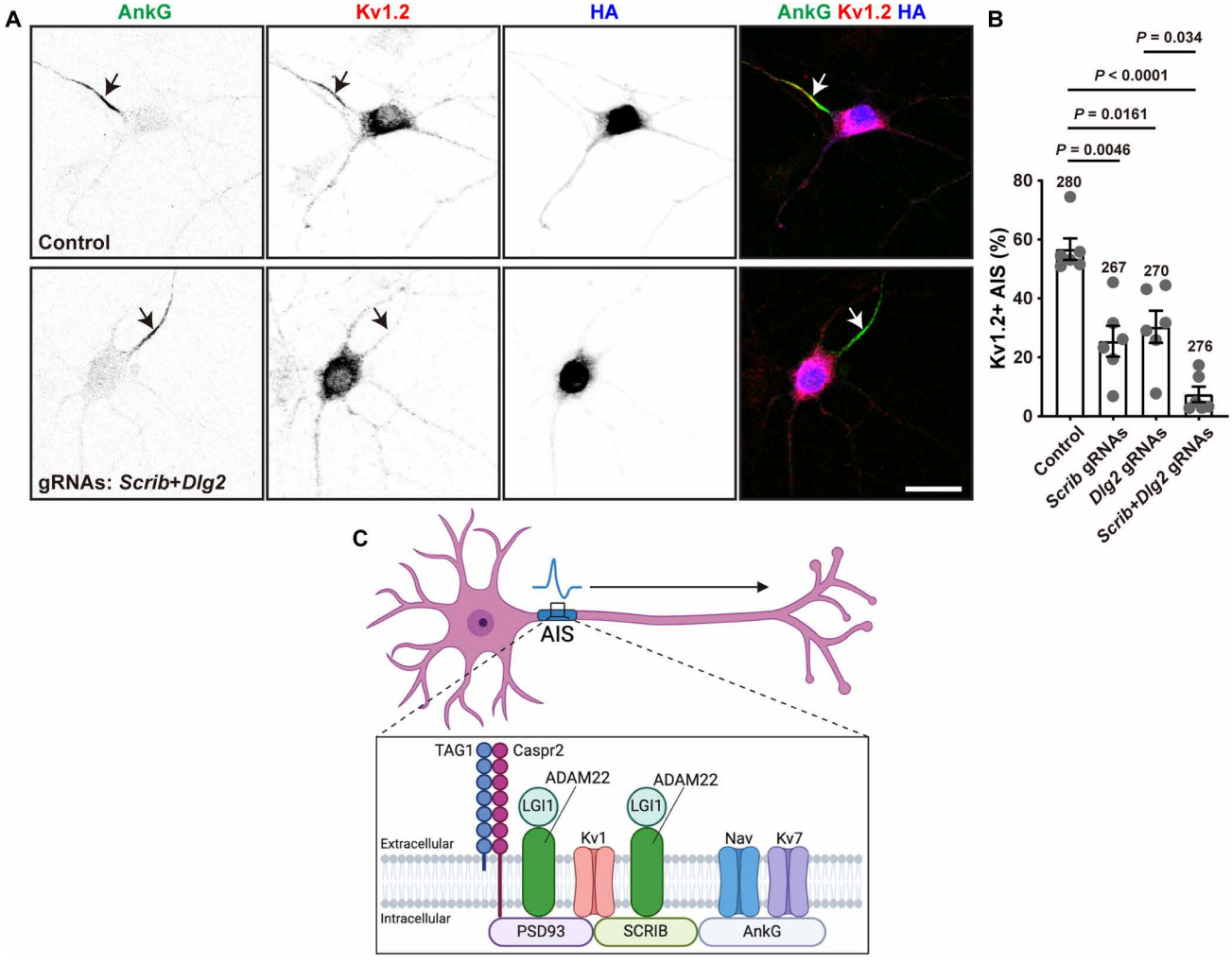

Fig. 8. SCRIB and PSD93 both contribute to AIS Kv1 channel clustering. (**A**) Immunostaining of hippocampal neurons using antibodies against AnkG (green), Kv1.2 (red), and HA (blue). AIS are indicated by arrows. Hippocampal neurons were transduced at DIV0 with Cas9 AAV and with AAV to express control plasmids or *Scrib+Dlg2* 3XgRNAs; both the control and 3XgRNA plasmids harbor an HA expression cassette. Neurons were fixed at DIV20. Scale bar, 20 μm. (**B**) Quantification of the number of HA+ neurons with Kv1.2+ AIS in hippocampal neurons transduced with control, *Scrib*, *Dlg2*, or *Scrib+Dlg2* 3XgRNAs. Hippocampal neurons were transduced at DIV0 and fixed at DIV20. The total number of neurons measured for each condition is shown on the graph. $N = 6$ for each experimental condition. Data are means ± SEM. Ordinary one-way ANOVA with Tukey's multiple comparisons test. (**C**) Cartoon illustrating the scaffolding protein complex and interactions responsible for AIS clustering of Kv1 channels, ADAM22, LGI1, Caspr2, and TAG1. Although both SCRIB and PSD93 can cluster and interact with Kv1 channels and ADAM22, only SCRIB binds to AnkG. Created in BioRender. M.N.R. (2025); https://BioRender.com/3q4w5px.

Our results do not rule out the possibility that extracellular interactions through ADAM22, Caspr2, TAG1, and LGI proteins may also participate in the stabilization of AIS Kv1 channel complexes. For example, AISs in the brain are enriched with many CAMs including NF186, NrCAM, and Contactin (*21*, *41*), and extracellular matrix molecules including Versican and Brevican (*42*); all of these depend directly or indirectly on AnkG for their AIS localization. Extracellular interactions may help explain the incomplete loss of Kv1 channels at the AIS after loss of SCRIB or PSD93 (Fig. 8B), and the complete loss of AIS Kv1 channels only after loss of both scaffolds. This may be consistent with the observation that loss of LGI1 reduces AIS Kv1 channel clustering (*18*).

AISs contain many different types of ion channels including Na^+, K^+, and Ca^{2+} channels (*1*). Among these, the most diversity exists in the types of AIS K^+ channels reflecting the importance of these channels to modulate action potential waveform and frequency of firing. These AIS K^+ channels include Kv1, Kv2, Kv7, and K2P channels. Although present in the AIS, Kv2 channels are found in clusters devoid of AnkG (*43*). Instead, AIS Kv2 channels interact with the vesicle-associated membrane protein–associated proteins isoforms A and B (VAPA and VAPB) for their clustering (*44*). Kv1, Kv7, and K2P channels all colocalize with AnkG at the AIS, and Kv7 and K2P channels also colocalize with AnkG at nodes of Ranvier (*9*, *10*, *45*). Among these AIS channels, only Kv7 and K2P channels have AnkG-binding motifs; the motif in Kv7 channels is nearly identical to the Ankyrin-binding motif found in all vertebrate Na^+ channels (*23*). The results presented here show that AIS Kv1 channel clustering depends on a hierarchy of three separate scaffolding proteins: AnkG, SCRIB, and PSD93. Among these, both PSD93 and SCRIB can interact with Kv1 channels and ADAM22. However, only SCRIB links Kv1

channels and ADAM22 to AnkG. Our results highlight not only the unique mechanisms responsible for AIS Kv1 channel clustering but also the core dependence on the master scaffolding protein AnkG.

MATERIALS AND METHODS

Animals

C57BL/6 mice were housed at Baylor College of Medicine and used for tissue collection. Timed pregnant Sprague-Dawley rats were purchased from Charles River Laboratories and housed at Baylor College of Medicine. Rats were euthanized for embryo collection at E18.5. $H11^{Cas9}$ CRISPR-Cas9 knock-in mice constitutively expressing the Cas9 endonuclease driven by the CAG promoter were purchased from the Jackson Laboratory (JAX mice, catalog no. 028239, RRID: IMSR_JAX: JAX: 028239) and maintained at Baylor College of Medicine. All animals were housed at 22°C temperature, 40~60% humidity, and a normal 12-hour light/12-hour dark schedule. Animals had access to food and water ad libitum. We did not consider sex as a variable in any of the experiments performed. All experiments involving animals were performed in compliance with the National Institutes of Health Guide for the Care and Use of Laboratory Animals and the Baylor College of Medicine Institutional Animal Care and Use Committee protocol no. AN-4634.

Antibodies

Primary antibodies used for immunofluorescence in this study were rabbit anti-SCRIB (ABclonal, catalog no. A17450, Lot: 0098460101, 1:100), mouse anti-PSD93 (NeuroMab, Clone N18/28, 1:200), mouse anti-AnkG (NeuroMab, Clone N106/65, 1:300), guinea pig anti-AnkG (SySy, catalog no. 386004, 1:1000), chicken anti-MAP2 (Encor, catalog no. CPCA-MAP2, 1:2000), mouse anti-Kv1.1 (NeuroMab, Clone K20/78, 1:200), mouse anti-Kv1.1 (NeuroMab, Clone K36/15, 1:200), mouse anti-Kv1.2 (NeuroMab, Clone K14/16, 1:200), mouse anti-Kvβ2 (NeuroMab catalog no. K17/70, RRID:AB_2131373, 1:200), rabbit anti-Kv1.4 N (1:50, a gift from J. Trimmer, UC Davis), mouse anti-ADAM22 (NeuroMab, catalog no. N57/2, RRID: AB_2223817, 1:200), mouse anti-PanNav (Sigma-Aldrich, catalog no. S8809, 1:500), guinea pig anti-TRIM46 (SySy, catalog no. 377005, 1:1000), guinea pig anti-TRIM46 (SySy, catalog no. 377308, 1:1000), mouse anti-FLAG (MBL International, catalog no. M185-3L, RRID:AB_1112-3930, 1:500), mouse anti-V5 (Invitrogen, catalog no. R960CUS, 1:500), rat anti-HA (Sigma-Aldrich, catalog no. 11867423001, 1:1000), rabbit anti-βIV spectrin (Rasband lab, 1:1000), rabbit anti-LGI1 (Abcam, catalog no. ab30868, RRID:AB_776017, 1:100), rabbit anti-Caspr2 [a gift from E. Peles, Weizmann Institute of Science, Rehovot, Israel, (*46*), 1:250], and goat polyclonal anti-TAG1 (R&D Systems, catalog no. AF4439, RRID:AB_2044647, 1:100). Fluorescent second antibodies used for immunocytochemistry in this study were goat anti-rabbit IgG (H+L) Alexa Fluor 488, goat anti-rabbit IgG (H+L) Alexa Fluor 594, goat anti-rabbit IgG (H+L) Alexa Fluor 647, goat anti-mouse IgG (H+L) Alexa Fluor PLUS 594, goat anti-chicken IgY 350, goat anti-guinea pig IgG (H+L) DyLight 350, goat anti-guinea pig IgG (H+L) Alexa Fluor 594, goat anti-guinea pig IgG (H+L) Alexa Fluor 647, goat anti-mouse IgG1 Alexa Fluor 488, goat anti-mouse IgG1 Alexa Fluor 594, goat anti-mouse IgG1 Alexa Fluor 647, goat anti-mouse IgG2a Alexa Fluor 488, goat anti-mouse IgG2a Alexa Fluor 594, goat anti-mouse IgG2b Alexa Fluor 488, goat anti-mouse IgG2b Alexa Fluor 594, goat anti-rat IgG (H+L) Alexa Fluor 594, and goat anti-rat IgG (H+L) Alexa Fluor 647. All second antibodies were from Invitrogen. goat anti-chicken IgY 350 and goat anti-guinea pig IgG (H+L) DyLight 350 were diluted as 1:200 for staining, whereas the rest were diluted as 1:1000.

Antibodies used for immunoblotting included rabbit anti-SCRIB (1:1000, catalog no. A17450, ABclonal), mouse anti-Kv1.1 (1:1000, Clone K36/15, NeuroMab), mouse anti-Kv1.2 (1:1000, Clone K14/16, NeuroMab), rabbit anti-Kv1.4 N (1:500, a gift from J. Trimmer, UC Davis), rabbit anti-Kv1.2 (J. Trimmer, University of California, Davis, catalog no. Kv1.2C, 1:1000), rabbit anti-βIV spectrin (1:1000, Rasband lab), rabbit anti-β-Tubulin (1:2000, catalog no. 2146, Cell Signaling), goat anti-mouse horseradish peroxidase (HRP) (1:4000, catalog no. 115-035-146, the Jackson Immunoresearch), goat anti-rabbit HRP (1:4000, catalog no. 111-035-003, the Jackson Immunoresearch), mouse anti-FLAG (MBL International, catalog no. M185-3L, 1:1000), rabbit anti-GFP (Thermo Fisher Scientific, catalog no. A11122, 1:1000), and rabbit anti-GFP (Proteintech, catalog no. 50430-2-AP, RRID:AB_11042881, 1:1000).

The antibodies used for immunoprecipitation included a mouse monoclonal against FLAG (Sigma-Aldrich, catalog no. F1804, RRID: AB_262044) and rabbit polyclonal antibodies against Kv1.4 N (J. Trimmer), SCRIB (ABclonal, catalog no. A17450, RRID:AB_2772164), and GFP (Thermo Fisher Scientific, catalog no. A11122, RRID: AB_221569).

Primary neuron culture

Hippocampal or cortical neurons were prepared from E18.5 Sprague-Dawley rat embryos. Dissected tissues were incubated in digestion solution for 20 min at 37°C: 0.25% trypsin for hippocampi and 0.25% trypsin and DNase (1 mg/ml) for chopped cortices. Dissociated hippocampal neurons were plated onto coverslips at a density of 12,000 cells/cm^2 in neuronal culture medium (Neurobasal medium, 2% B-27 supplement, 1% Glutamax-I, and 1% penicillin-streptomycin). Cortical neurons were plated onto coverslips at a density of 36,000 cells/cm^2, whereas in 6-well plates, they were plated at a density of 400,000 cells/cm^2. Coverslips were coated sequentially using poly-D-lysine (PDL; 1 mg/ml; Sigma-Aldrich, catalog no. P7886-1G) and laminin mouse protein (10 μg/ml; Gibco, catalog no. 23017015). Six-well plates were coated using PDL (1 mg/ml), and neurons grown on the plates were used for immunoblotting studies. After plating neurons for 3 hours, the medium was changed. To slow glial cell proliferation, we added 2 μM cytosine β-D-arabinofuranoside hydrochloride (AraC) to DIV6 neurons in 6-well plates. Every 6 days, one-third of the medium was replaced with fresh neuronal culture medium. Neurons were fixed or harvested at indicated time points.

Cell lines

HEK293T cells or COS7 cells were grown in Dulbecco's modified Eagle's medium (DMEM) complete medium with 10% fetal bovine serum (FBS), 1% penicillin-streptomycin, and 1% Glutamax-I. Passaging was performed when cells reached confluency.

Bioinformatics

PDZ domain-containing proteins were identified using UniProt. The search was refined by using the rat proteome ID UP000002494 and PDZ domain. After removing noncanonical isoforms, 144 PDZ domain-containing proteins were identified. The list of PDZ domain-containing proteins found in our AIS proteome was generated from

the top 1000 proteins from the DIV14 IPL-AIS dataset (*20*). The Pfam protein domain database was referenced to identify the number of PDZ domains for each protein.

CRISPR-Cas9–mediated smFP-V5 tag knock-in

We used homology-independent repair to tag the following rat genes: *Magi3*, *Pdzd2*, *Scrib*, *Dlg2*, *Prex1*, *Nos1*, *Mast1*, *Deptor*, *Arhgap21*, *Cnksr2*, *Ahnak*, *Lrrc7*, *Tiam1*, *Myo18a*, *Afdn*, *Shank1*, *Rapgef2*, and *Pick1* and mouse *Sptbn4* and *Scrib* as previously described (*21*). Ours is a modified strategy based on the HiUGE method (*20*–*22*). Briefly, knock-in plasmids harboring two cassettes including U6 promoters, a GS-gRNA and a donor-specific gRNA (DS-gRNA); smFP-V5 tag oligonucleotides were flanked by donor recognition sites (DRSs); the above DNA sequences were flanked by two inverted terminal repeats (ITRs). Knock-in plasmids were constructed by inserting GS-gRNAs as paired oligonucleotides into the *BbsI* linearized plasmid R2O2: smFP-V5. GS-gRNAs targeting the last exon of candidate genes were designed using CRISPOR (*47*).

In vitro knock-in was performed in primary neurons transduced with AAVs. Three plasmids were used for AAV production: AAV plasmid, helper plasmid, and serotype PHP.S plasmid. AAV plasmids were the knock-in plasmids or pAAV-SpCas9. HEK293T cells were transfected with the three plasmids using PEI MAX, followed by a medium change after 18 hours. Cell lysates were collected from 12-well plates after 3 days of transfection. The titer of AAVs was 3×10^{10} to 1×10^{11} copies/ml. Cortical or hippocampal rat neurons were transduced at DIV1 to DIV2 with 20 μl of AAVs consisting of 10 μl of Cas9 and 10 μl of knock-in AAVs. Neuronal culture medium was changed after 2 days. Two weeks later, samples were fixed and used for immunocytochemistry.

In vivo knock-in was performed in adult Cas9 transgenic mice using intravitreal injection of purified AAV. HEK293T cells were transfected with three plasmids: AAV plasmid, helper plasmid, and pAAV-RC using PEI MAX in eight 15 cm dishes, followed by a medium change after 18 hours. After 3 days of transfection, AAV were extracted from transfected HEK293T cells, purified, and concentrated using the AAVpro Purification Kit Maxi (catalog no. 6666, Takara). Cas9 mice were anesthetized and injected with 2 μl of ~1×10^{12} copies/ml AAVs per eye. After 3 weeks, retinas and optic nerves were dissected and used for immunohistochemistry.

CRISPR-Cas9–mediated gene disruption

CRISPR-Cas9–mediated gene disruption was performed as previously described (*20*, *21*). Briefly, the plasmid knockout backbone pAAV-3XU6 harbors three cassettes for GS-gRNAs (3XgRNAs) driven by the U6 promoter, an smFP-HA that includes 10XHA tags driven by neuron-specific human synapsin 1 promoter, and the above DNA sequences were flanked by ITRs. The smFP-HA was used as reporter to identify transduced neurons. Besides template plasmids, we used five 3XgRNAs plasmids targeting rat *Scrib*, mouse *Scrib*#1, mouse *Scrib*#2, rat *Ank3*, and rat *Dlg2*. 3XgRNAs for rat *Dlg2* and mouse *Scrib* were designed using CRISPOR (*47*). 3XgRNAs targeting rat *Scrib* and rat *Ank3* were described previously (*20*).

Primary rat neurons were transduced at DIV0 to DIV2 using Cas9 AAV together with template control AAVs or 3XgRNAs AAVs. Briefly, 20 μl of AAVs consisting of 10 μl of Cas9 AAV and 10 μl of template or knockout AAVs were added to 12-well plates. The neuronal culture medium was changed after 2 days. Neurons were fixed at DIV14 or DIV20 and used for immunolabeling. In the case of simultaneous targeting of both *Scrib* and *Dlg2*, both knockout AAVs were added in the same well and at the same time.

Immunoblotting

Cortical rat neurons in 6-well plates were transduced with 25 μl of AAVs of template or rat *Scrib* 3XgRNAs AAV together with 25 μl of Cas9 AAV at DIV1. Transduced neurons were lysed at DIV20 with cell lysis solution containing 50 mM tris-HCl (pH 7.6), 150 mM NaCl, 1% SDS, 0.5% sodium deoxycholate, 1% Triton X-100, and a protease inhibitor cocktail. Lysed samples were placed on ice for 10 min, heated at 95°C for 10 min, and sonicated on ice. Supernatants were collected and heated at 95°C for 10 min with reducing sample buffer including 62.5 mM tris-HCl (pH 6.8), 2% SDS, 10% glycerol, 2% 2-mercaptoethanol, and 0.005% bromophenol blue (GenDEPOT, catalog no. L1100). Proteins were loaded in 4 to 15% polyacrylamide gels. The SDS–polyacrylamide gel electrophoresis gels were run at 120-V constant voltage in Tris-glycine-SDS running buffer and transferred to 0.45-μm nitrocellulose membranes (Bio-Rad, catalog no. 1620115) at 240-mA constant current in Tris-glycine-methanol transfer buffer. The blots were blocked with 5% (w/v) nonfat dried milk in PBS for 1 hour at room temperature (RT). Primary antibodies were incubated overnight at 4°C. HRP-conjugated secondary antibodies were incubated for 1 hour at RT. TBST [20 mM tris-HCl (pH 7.4), 150 mM NaCl, and 0.1% Tween 20] was used for membrane washing and antibody dilution. The blots were visualized using a SuperSignal West Pico PLUS Chemiluminescent Substrate (Thermo Fisher Scientific, catalog no. 34580) and imaged in a LI-COR Odyssey imaging system.

Immunofluorescence of neurons

Primary neurons were fixed in 4% PFA on ice for 15 min and washed three times in 0.1 M phosphate buffer (PB). Blocking was performed for 1 hour at RT in PBTGS (10% normal goat serum and 0.3% Triton X-100 in 0.1 M PB). Then, samples were incubated with primary antibodies diluted in PBTGS for 1 or 1.5 hours at RT. After washing three times in PBTGS, secondary antibodies were added for 1 hour at RT. After washing in 0.1 M PB, coverslips were mounted on the slides using a VECTASHIELD Vibrance Antifade Mounting Medium (Vector Laboratories, catalog no. H-1700-10). In some cases, we detergent extracted DIV21 or DIV27 hippocampal neurons with ice-cold 1X phosphate-buffered saline (PBS) containing 0.5% Triton X-100 at 4°C for 30 min and then washed three times in ice-cold PBS at 4°C, followed by fixation with 4% PFA (pH 7.2) for 15 min at 4°C.

For immunostaining of brain sections, adult mice were deeply anesthetized with isoflurane and perfused transcardially with PBS and cold 4% PFA/15% picric acid solution (pH 7.3) sequentially, followed by a 2-hour postfixation in cold 4% PFA/15% picric acid solution. PFA was dissolved in 0.1 M PB. No perfusion was performed for P1 and P4 mice, and their brains were directly dissected out and immersed in cold 4% PFA/15% picric acid solution for 2 hours. Sciatic or optic nerves were dissected out from perfused adult mice. Fixed brains or nerves were dehydrated in 30% sucrose in 0.1 M PB at 4°C for 2 days. Brains were sectioned at 20 μm, and nerves were sectioned at 10 μm.

Antigen retrieval was performed before brain tissue staining. Brain coronal sections or nerves were heated at 95°C for 15 min in pH 8 sodium citrate buffer. Samples were blocked for 2 hours at RT in PBTGS. Primary antibodies were incubated overnight at 4°C. After washing three times, sections were incubated in fluorescent secondare antibodies for 1 hour at RT. Nuclei were counterstained with

Hoechst 33258 (Invitrogen, catalog no. H3569). Washed tissues were mounted on the slides using a VECTASHIELD Vibrance Antifade Mounting Medium (Vector Laboratories, catalog no. H-1700-10).

Microscopy

Images were acquired using a Zeiss upright structured illumination microscope with Apotome 2. Primary neurons and cells were imaged using 40x air objective with 0.95 numerical aperture. Brain and nerve sections were imaged using 40x air objective with 0.95 numerical aperture or 63x and 100x oil objective with 1.4 numerical aperture. *Z*-stacks with 0.5-μm step size were used for imaging. *Z*-projection and image adjustments were performed using Fiji-ImageJ or Adobe Photoshop; all adjustments to lookup tables were linear. Figures were prepared using Adobe Illustrator.

Super-resolution microscopy

For STED experiments, DIV22 primary hippocampal neurons were treated with ice-cold 1X PBS containing 0.5% Triton X-100 for 30 min at 4°C. After three 5-min washes with ice-cold PBS, neurons were fixed with 4% PFA (pH 7.2) for 15 min at 4°C and then washed again three times in 1X PBS. Blocking was performed for 1 hour at RT in PBTGS, followed by primary antibody incubation overnight at 4°C. The following primary antibodies were diluted 1:100 in PBTGS: rabbit anti-SCRIB (ABclonal, catalog no. A17450), mouse anti-Kv1.1 (NeuroMab, Clone K36/15), and mouse anti-PSD93 (NeuroMab, Clone N18/28). Neurons were then washed three times in PBTGS and incubated with secondary antibodies diluted 1:300 in PBTGS for 2 hours at RT. The following secondary antibodies were used: goat anti-mouse STAR-RED (Abberior, catalog no. STRED-1001-500UG) and goat anti-rabbit STAR-ORANGE (Abberior, catalog no. STORANGE-1002-500UG). After secondary antibody incubation, neurons were washed three times in 0.1 M PB, followed by three washes in 0.05 M PB. Coverslips were mounted with Abberior Liquid Antifade mounting media (catalog no. MM-2009-2X15ML).

STED imaging was performed using an Abberior STEDYCON system fitted to a Nikon Eclipse Ti2 microscope. Images were acquired with a Plan Apochromat 100x oil immersion objective with a numerical aperture of 1.45. Images were deconvolved using a standard deconvolution profile in Huygens Essential Version 24.10 (Scientific Volume Imaging, The Netherlands; http://svi.nl). Maximum intensity *Z*-projections of deconvolved images were generated and analyzed in Fiji-ImageJ. To quantify the periodic organization of SCRIB, Kv1.1, and PSD93, fluorescence intensities were measured from a line drawn along the AIS. The distance between peak fluorescence intensities (maximum to maximum) was calculated and averaged for each AIS line profile.

For STORM experiments, rat hippocampal neurons cultured on #1.5H coverslips (Neuvitro) were detergent extracted at 14 days in vitro in PEM [80 mM PIPES, 5 mM EGTA, and 2 mM $MgCl_2$ (pH 6.8)] containing 0.5% Triton X-100 for 5 min at RT and then fixed for 10 min at RT in 4% PFA in PEM. They were then washed three times with 0.1 M PB, blocked for 1 hour in blocking buffer (0.1 M PB containing 0.22% bovine gelatin and 0.1% Triton X-100), and incubated overnight at 4°C with primary antibodies diluted in blocking buffer [rabbit anti-SCRIB (ABclonal, catalog no. A17450, 1:100) and chicken anti-Neurofascin (R&D Systems, catalog no. AF3235, 1:1000)]. The coverslip was then washed with blocking buffer, incubated for 1 hour at RT with secondary antibodies diluted in blocking buffer (goat anti-rabbit Alexa Fluor 647, 1:300, and goat anti-chicken Alexa Fluor 488, 1:1000) and then washed with blocking buffer and 0.1 M PB. The coverslip was imaged in a Smart Kit Buffer (Abbelight) on an N-STORM microscope (Nikon Instruments). The sample was illuminated with a 640-nm laser at full power with progressive reactivation by simultaneous 405-nm illumination, and 40,000 images were collected at 109 Hz. Nikon Elements N-STORM software was used to compute single molecule localizations. Image reconstruction (16 nm/pixel) was performed in Fiji-ImageJ using the ThunderSTORM and ChriSTORM plugins, and an 8-nm Gaussian blur was applied (*28*, *48*).

Surface clustering assay

COS7 cells were seeded at a low density (30 to 40% confluent at time of transfection) on PDL-coated coverslips and transfected with plasmid DNA using Lipofectamine 3000 (Thermo Fisher Scientific, catalog no. L300015) according to the manufacturer's instructions. Twenty-four hours after transfection, cells were fixed with 4% PFA (pH 7.2) for 30 min at 4°C and washed three times with 1X PBS. Cells were permeabilized and blocked with PBTGS for 1 hour at RT and then stained with primary antibodies diluted in PBTGS for 1 hour at RT. After three washes with PBTGS, cells were incubated with secondary antibodies diluted in PBTGS for 1 hour. The coverslips were washed with PBTGS and then PB before they were mounted on slides. To detect surface Kv1.1, an antibody that recognizes the extracellular domain of Kv1.1 (UC Davis/NIH NeuroMab Facility, catalog no. K36/15, RRID:AB_2877294) was used. Primary and secondary antibodies were diluted in cold culture media [high-glucose DMEM (Gibco, catalog no. 11965092) supplemented with 10% FBS, 1X penicillin-streptomycin (Gibco, catalog no. 15140122), and 1X GlutaMAX (Gibco, catalog no. 35050061)] and added to live cells for 30 min on ice, with cold PBS washes following each incubation. The cells were then fixed, permeabilized, and stained with cytoplasmically directed antibodies as described above. Three independent experiments were performed for each transfection condition, and representative images are shown in the figures.

For the surface clustering assays and immunoprecipitation (see below), the following plasmids were used: pcDNA3 (Thermo Fisher Scientific), RBG4-Kv1.1 (RRID:Addgene_196943), RBG4-Kv1.2 (RRID:Addgene_196941), RBG4-Kv1.4 (RRID:Addgene_196938), pGW-PSD93-EGFP (a gift from B. Firestein, Rutgers, Piscataway, NJ, USA), AnkG270-EGFP (a gift from V. Bennett, Duke University, Durham, NC, USA), pcDNA3-SCRIB-FLAG, and pSCT-ADAM22. The generation of pcDNA3-SCRIB-FLAG (*20*) and pSCT-ADAM22 (*15*) was previously described. All plasmids were verified by whole plasmid sequencing (Plasmidsaurus). Kv1.4ΔPDZ was generated by mutagenizing RBG4-Kv1.4 using In-Fusion Cloning (Takara Bio) and the following primers: 5′-AGGCTGTGTGAATCTCTTTCCCCACCTGCC-3′ and 5′-AGA TTCACACAGCCTTTGCATTAGAACAGTTG-3′.

Successful deletion of the PDZ-binding motif was verified by Sanger sequencing (GENEWIZ).

Immunoprecipitation

HEK293T cells were seeded on PDL-coated plates to reach 70 to 80% confluency at time of transfection. A half-media change was performed a half hour prior to transfection with plasmid DNA. Cells were transfected using Lipofectamine 3000 (Invitrogen, catalog no. L300015) as per the manufacturer's instructions, and a full media change was performed the following day. Two days after transfection, cells were washed in ice-cold 1X PBS and then solubilized with lysis

buffer [20 mM tris-HCl (pH 8.0), 150 mM NaCl, 1% (v/v) Triton X-100, 10 mM EDTA (pH 8.0), 10 mM NaN_3, 0.5 mM phenylmethylsulfonyl fluoride, and 1X protease inhibitor cocktail] for 15 min on ice. The lysates were transferred to chilled tubes, rotated for 10 min at 4°C, and centrifuged at 14,000*g* for 10 min at 4°C. The supernatants were collected, and protein concentration was measured with a BCA assay (Bio-Rad). A 300-μg lysate was rotated overnight at 4°C with 1 μl of FLAG M2 antibody (Sigma-Aldrich, catalog no. F1804, RRID: AB_262044), 3 μl of Kv1.4 antibody (J. Trimmer), 1.5 μl of SCRIB antibody (ABclonal, catalog no. A17450, RRID:AB_2772164), or 1.5 μl of GFP antibody (Thermo Fisher Scientific, catalog no. A11122, RRID: AB_221569). The next day, Protein G (Cytiva, catalog no. 28951379) or Protein A (Cytiva, catalog no. 28951378) magnetic Sepharose beads was washed twice with lysis buffer and then blocked with 0.1% (w/v) bovine serum albumin in lysis buffer for 1 hour at 4°C, rotating. The beads were washed twice with lysis buffer, added to the lysate-antibody mixture, and rotated for 1 hour at 4°C. The beads were then washed seven times with lysis buffer to remove unbound proteins. Following the final wash, any remaining lysis buffer was removed, and the beads were resuspended in reducing sample buffer and incubated for 5 min at 95°C. Input and immunoprecipitated samples were assessed by immunoblot using a LI-COR Odyssey Fc Imaging System. Adobe Photoshop was used to make linear contrast adjustments and to crop images. Three independent experiments were performed for each co-IP, and representative images are shown in the figures.

MEA recordings

MEA recordings were performed as previously described (*49*) with slight modifications. Briefly, 96-well CytoView MEA plates (Axion Biosystems, #M768-tMEA-96W-5) were coated with poly-L-lysine (1 mg/ml; Sigma-Aldrich, catalog no. P2636) in borate buffer (pH 8.5) overnight. Neonatal H11-Cas9 mice (JAX mice, catalog no. 027650) were euthanized by decapitation, and forebrain tissue was rapidly isolated and dissociated with papain. Cells were seeded as droplets onto the MEA plates (~150,000 cells per well) and maintained in Neurobasal Plus medium (Thermo Fisher Scientific, catalog no. A3653401). AAVs expressing *mScrib*-KO gRNA or nontargeting controls were applied on DIV1 at a normalized amount of 1×10^8 copies per well. Recordings were conducted using a Maestro Pro MEA system on DIV8, DIV11, and DIV14 and then analyzed using an AxIS Navigator (Axion Biosystems). Single electrode bursts were defined as a minimum of five spikes, separated by an interspike interval (ISI) of no more than 100 ms. Network bursts were defined as a minimum of 50 spikes, separated by an ISI of no more than 100 ms with at least 35% participating electrodes.

Measurement of AIS fluorescence intensities and the polarity index

To determine the AIS fluorescence intensity, a 10-pixel-wide line was drawn along the AIS and the integrated intensity of AIS fluorescence was measured using Fiji-ImageJ. The corrected total fluorescence (CTF) for any given AIS protein was obtained by using integrated intensity minus background of the same size. CTF normalization was performed against control samples. Transduced neurons with epitope-tagged PDZ domain-containing proteins were used for the polarity index analysis; βIV spectrin was used to identify the AIS, and the same region was used to measure the AIS V5 tag signal. Briefly, a 10-pixel-wide line was drawn along the AIS or along proximal and similar width dendrites in Fiji-ImageJ. The background was also measured in the same image. We used the corrected mean intensity fluorescence (CMF; mean intensity of the AIS or dendrites minus background) ratio of the AIS and dendrites to evaluate the polarity distribution. The polarity index is defined as AIS CMF/Dendrite CMF.

Statistics

All statistical analyses were performed using GraphPad Prism 8. The statistical details including the number of experiments, number of cells, and statistical tests can be found in the figure legends. Data distribution was assumed to be normal, although this was not formally tested. Statistical analysis was performed by unpaired two-tailed *t* test followed by Welch's correction for two group comparisons and by one-way analysis of variance (ANOVA) for multiple group comparisons. Graphs are presented as the means ± SEM. Differences were considered significant when *P* values were less than 0.05.

Supplementary Materials

The PDF file includes:
Figs. S1 to S4
Legend for data S1

Other Supplementary Material for this manuscript includes the following:
Data S1

REFERENCES AND NOTES

1. C. Leterrier, The axon initial segment: An updated viewpoint. *J. Neurosci.* **38**, 2135–2145 (2018).
2. A. Lorincz, Z. Nusser, Cell-type-dependent molecular composition of the axon initial segment. *J. Neurosci.* **28**, 14329–14340 (2008).
3. M. H. P. Kole, J. J. Letzkus, G. J. Stuart, Axon initial segment Kv1 channels control axonal action potential waveform and synaptic efficacy. *Neuron* **55**, 633–647 (2007).
4. L. N. Manganas, J. S. Trimmer, Subunit composition determines Kv1 potassium channel surface expression. *J. Biol. Chem.* **275**, 29685–29693 (2000).
5. K. J. Rhodes, B. W. Strassle, M. M. Monaghan, Z. Bekele-Arcuri, M. F. Matos, J. S. Trimmer, Association and colocalization of the Kvβ1 and Kvβ2 β-subunits with Kv1 α-subunits in mammalian brain K^+ channel complexes. *J. Neurosci.* **17**, 8246–8258 (1997).
6. C. Villa, R. Combi, Potassium channels and human epileptic phenotypes: An updated overview. *Front. Cell. Neurosci.* **10**, 81 (2016).
7. G. Lemaillet, B. Walker, S. Lambert, Identification of a conserved ankyrin-binding motif in the family of sodium channel α subunits. *J. Biol. Chem.* **278**, 27333–27339 (2003).
8. J. J. Garrido, P. Giraud, E. Carlier, F. Fernandes, A. Moussif, M.-P. Fache, D. Debanne, B. Dargent, A targeting motif involved in sodium channel clustering at the axonal initial segment. *Science* **300**, 2091–2094 (2003).
9. Z. Pan, T. Kao, Z. Horvath, J. Lemos, J.-Y. Sul, S. D. Cranstoun, V. Bennett, S. S. Scherer, E. C. Cooper, A common ankyrin-G-based mechanism retains KCNQ and Na_v channels at electrically active domains of the axon. *J. Neurosci.* **26**, 2599–2613 (2006).
10. G. Escobedo Jr., Y. Wu, Y. Ogawa, X. Ding, M. N. Rasband, An evolutionarily conserved AnkyrinG-dependent motif clusters axonal K2P K^+ channels. *J. Cell Biol.* **223**, e202401140 (2024).
11. V. Luque-Fernández, S. K. Vanspauwen, A. Landra-Willm, E. Arvedsen, M. Besquent, G. Sandoz, H. B. Rasmussen, An ankyrin G-binding motif mediates TRAAK periodic localization at axon initial segments of hippocampal pyramidal neurons. *Proc. Natl. Acad. Sci. U.S.A.* **121**, e2310120121 (2024).
12. D. Sánchez-Ponce, J. DeFelipe, J. J. Garrido, A. Muñoz, Developmental expression of Kv potassium channels at the axon initial segment of cultured hippocampal neurons. *PLOS ONE* **7**, e48557 (2012).
13. E. Kim, M. Niethammer, A. Rothschild, Y. N. Jan, M. Sheng, Clustering of Shaker-type K^+ channels by interaction with a family of membrane-associated guanylate kinases. *Nature* **378**, 85–88 (1995).
14. A. M. Tiffany, L. N. Manganas, E. Kim, Y. P. Hsueh, M. Sheng, J. S. Trimmer, PSD-95 and SAP97 exhibit distinct mechanisms for regulating K^+ channel surface expression and clustering. *J. Cell Biol.* **148**, 147–158 (2000).
15. Y. Ogawa, J. Oses-Prieto, M. Y. Kim, I. Horresh, E. Peles, A. L. Burlingame, J. S. Trimmer, D. Meijer, M. N. Rasband, ADAM22, a Kv1 channel-interacting protein, recruits

membrane-associated guanylate kinases to juxtaparanodes of myelinated axons. *J. Neurosci.* **30**, 1038–1048 (2010).
16. Y. Ogawa, I. Horresh, J. S. Trimmer, D. S. Bredt, E. Peles, M. N. Rasband, Postsynaptic density-93 clusters Kv1 channels at axon initial segments independently of Caspr2. *J. Neurosci.* **28**, 5731–5739 (2008).
17. A. Duflocq, F. Chareyre, M. Giovannini, F. Couraud, M. Davenne, Characterization of the axon initial segment (AIS) of motor neurons and identification of a para-AIS and a juxtapara-AIS, organized by protein 4.1B. *BMC Biol.* **9**, 66 (2011).
18. M. Seagar, M. Russier, O. Caillard, Y. Maulet, L. Fronzaroli-Molinieres, M. De San Feliciano, N. Boumedine-Guignon, L. Rodriguez, M. Zbili, F. Usseglio, C. Formisano-Tréziny, F. Youssouf, M. Sangiardi, M. Boillot, S. Baulac, M. J. Benitez, J.-J. Garrido, D. Debanne, O. El Far, LGI1 tunes intrinsic excitability by regulating the density of axonal Kv1 channels. *Proc. Natl. Acad. Sci. U.S.A.* **114**, 7719–7724 (2017).
19. B. Hivert, L. Marien, K. N. Agbam, C. Faivre-Sarrailh, ADAM22 and ADAM23 modulate the targeting of the Kv1 channel-associated protein LGI1 to the axon initial segment. *J. Cell Sci.* **132**, jcs219774 (2019).
20. W. Zhang, Y. Fu, L. Peng, Y. Ogawa, X. Ding, A. Rasband, X. Zhou, M. Shelly, M. N. Rasband, P. Zou, Immunoproximity biotinylation reveals the axon initial segment proteome. *Nat. Commun.* **14**, 8201 (2023).
21. Y. Ogawa, B. C. Lim, S. George, J. A. Oses-Prieto, J. M. Rasband, Y. Eshed-Eisenbach, H. Hamdan, S. Nair, F. Boato, E. Peles, A. L. Burlingame, L. Van Aelst, M. N. Rasband, Antibody-directed extracellular proximity biotinylation reveals that Contactin-1 regulates axo-axonic innervation of axon initial segments. *Nat. Commun.* **14**, 6797 (2023).
22. Y. Gao, E. Hisey, T. W. A. Bradshaw, E. Erata, W. E. Brown, J. L. Courtland, A. Uezu, Y. Xiang, Y. Diao, S. H. Soderling, Plug-and-play protein modification using homology-independent universal genome engineering. *Neuron* **103**, 583–597.e8 (2019).
23. A. S. Hill, A. Nishino, K. Nakajo, G. Zhang, J. R. Fineman, M. E. Selzer, Y. Okamura, E. C. Cooper, Ion channel clustering at the axon initial segment and node of ranvier evolved sequentially in early chordates. *PLOS Genet.* **4**, e1000317 (2008).
24. M. N. Rasband, The axon initial segment and the maintenance of neuronal polarity. *Nat. Rev. Neurosci.* **11**, 552–562 (2010).
25. I. Horresh, S. Poliak, S. Grant, D. Bredt, M. N. Rasband, E. Peles, Multiple molecular interactions determine the clustering of Caspr2 and Kv1 channels in myelinated axons. *J. Neurosci.* **28**, 14213–14222 (2008).
26. S. Berghs, D. Aggujaro, R. Dirkx Jr., E. Maksimova, P. Stabach, J. M. Hermel, J. P. Zhang, W. Philbrick, V. Slepnev, T. Ort, M. Solimena, βIV spectrin, a new spectrin localized at axon initial segments and nodes of ranvier in the central and peripheral nervous system. *J. Cell Biol.* **151**, 985–1002 (2000).
27. K. Xu, G. Zhong, X. Zhuang, Actin, spectrin, and associated proteins form a periodic cytoskeletal structure in axons. *Science* **339**, 452–456 (2013).
28. C. Leterrier, J. Potier, G. Caillol, C. Debarnot, F. Rueda Boroni, B. Dargent, Nanoscale architecture of the axon initial segment reveals an organized and robust scaffold. *Cell Rep.* **13**, 2781–2793 (2015).
29. L. N. Manganas, Q. Wang, R. H. Scannevin, D. E. Antonucci, K. J. Rhodes, J. S. Trimmer, Identification of a trafficking determinant localized to the Kv1 potassium channel pore. *Proc. Natl. Acad. Sci. U.S.A.* **98**, 14055–14059 (2001).
30. P. Humbert, S. Russell, H. Richardson, Dlg, Scribble and Lgl in cell polarity, cell proliferation and cancer. *Bioessays* **25**, 542–553 (2003).
31. D. Bilder, M. Li, N. Perrimon, Cooperative regulation of cell polarity and growth by *Drosophila* tumor suppressors. *Science* **289**, 113–116 (2000).
32. M. M. Moreau, N. Piguel, T. Papouin, M. Koehl, C. M. Durand, M. E. Rubio, F. Loll, E. M. Richard, C. Mazzocco, C. Racca, S. H. R. Oliet, D. N. Abrous, M. Montcouquiol, N. Sans, The planar polarity protein Scribble1 is essential for neuronal plasticity and brain function. *J. Neurosci.* **30**, 9738–9752 (2010).
33. J. Szczurkowska, A. Guo, J. Martin, S.-I. Lee, E. Martinez, C. T. Chien, T. A. Khan, R. Singh, D. Dadson, T. S. Tran, S. Pautot, M. Shelly, Semaphorin3A/PlexinA3 association with the Scribble scaffold for cGMP increase is required for apical dendrite development. *Cell Rep.* **38**, 110483 (2022).
34. M. Fanciulli, L. Santulli, L. Errichiello, C. Barozzi, L. Tomasi, L. Rigon, T. Cubeddu, A. de Falco, A. Rampazzo, R. Michelucci, S. Uzzau, S. Striano, F. A. de Falco, P. Striano, C. Nobile, LGI1 microdeletion in autosomal dominant lateral temporal epilepsy. *Neurology* **78**, 1299–1303 (2012).
35. M. M. van der Knoop, R. Maroofian, Y. Fukata, Y. van Ierland, E. G. Karimiani, A. E. Lehesjoki, M. Muona, A. Paetau, Y. Miyazaki, Y. Hirano, L. Selim, M. de França, R. A. Fock, C. Beetz, C. A. L. Ruivenkamp, A. J. Eaton, F. D. Morneau-Jacob, L. Sagi-Dain, L. Shemer-Meiri, A. Peleg, J. Haddad-Halloun, D. J. Kamphuis, C. M. P. C. D. Peeters-Scholte, S. H. Kurul, R. Horvath, H. Lochmüller, D. Murphy, S. Waldmuller, S. Spranger, D. Overberg, A. M. Muir, A. Rad, B. Vona, F. Abdulwahad, S. Maddirevula, I. S. Povolotskaya, V. Y. Voinova, V. K. Gowda, V. M. Srinivasan, F. S. Alkuraya, H. C. Mefford, M. Alfadhel, T. B. Haack, P. Striano, M. Severino, M. Fukata, Y. Hilhorst-Hofstee, H. Houlden, Biallelic ADAM22 pathogenic variants cause progressive encephalopathy and infantile-onset refractory epilepsy. *Brain* **145**, 2301–2312 (2022).
36. K. A. Strauss, E. G. Puffenberger, M. J. Huentelman, S. Gottlieb, S. E. Dobrin, J. M. Parod, D. A. Stephan, D. H. Morton, Recessive symptomatic focal epilepsy and mutant contactin-associated protein-like 2. *N. Engl. J. Med.* **354**, 1370–1377 (2006).
37. K. R. Senechal, C. Thaller, J. L. Noebels, ADPEAF mutations reduce levels of secreted LGI1, a putative tumor suppressor protein linked to epilepsy. *Hum. Mol. Genet.* **14**, 1613–1620 (2005).
38. K. Konno, M. Yamasaki, T. Miyazaki, M. Watanabe, Glyoxal fixation: An approach to solve immunohistochemical problem in neuroscience research. *Sci. Adv.* **9**, eadf7084 (2023).
39. M. N. Rasband, E. W. Park, D. Zhen, M. I. Arbuckle, S. Poliak, E. Peles, S. G. N. Grant, J. S. Trimmer, Clustering of neuronal potassium channels is independent of their interaction with PSD-95. *J. Cell Biol.* **159**, 663–672 (2002).
40. N. Kozar-Gillan, A. Velichkova, G. Kanatouris, Y. Eshed-Eisenbach, G. Steel, M. Jaegle, E. Aunin, E. Peles, C. Torsney, D. N. Meijer, LGI3/2-ADAM23 interactions cluster Kv1 channels in myelinated axons to regulate refractory period. *J. Cell Biol.* **222**, e202211031 (2023).
41. A. D. Nelson, P. M. Jenkins, Axonal membranes and their domains: Assembly and function of the axon initial segment and node of Ranvier. *Front. Cell. Neurosci.* **11**, 136 (2017).
42. K. Susuki, K. J. Chang, D. R. Zollinger, Y. Liu, Y. Ogawa, Y. Eshed-Eisenbach, M. T. Dours-Zimmermann, J. A. Oses-Prieto, A. L. Burlingame, C. I. Seidenbecher, D. R. Zimmermann, T. Oohashi, E. Peles, M. N. Rasband, Three mechanisms assemble central nervous system nodes of Ranvier. *Neuron* **78**, 469–482 (2013).
43. P. D. Sarmiere, C. M. Weigle, M. M. Tamkun, The Kv2.1 K^+ channel targets to the axon initial segment of hippocampal and cortical neurons in culture and in situ. *BMC Neurosci.* **9**, 112 (2008).
44. M. Kirmiz, N. C. Vierra, S. Palacio, J. S. Trimmer, Identification of VAPA and VAPB as Kv2 channel-interacting proteins defining endoplasmic reticulum-plasma membrane junctions in mammalian brain neurons. *J. Neurosci.* **38**, 7562–7584 (2018).
45. J. J. Devaux, K. A. Kleopa, E. C. Cooper, S. S. Scherer, KCNQ2 is a nodal K^+ channel. *J. Neurosci.* **24**, 1236–1244 (2004).
46. S. Poliak, D. Salomon, H. Elhanany, H. Sabanay, B. Kiernan, L. Pevny, C. L. Stewart, X. Xu, S.-Y. Chiu, P. Shrager, A. J. W. Furley, E. Peles, Juxtaparanodal clustering of Shaker-like K^+ channels in myelinated axons depends on Caspr2 and TAG-1. *J. Cell Biol.* **162**, 1149–1160 (2003).
47. J. P. Concordet, M. Haeussler, CRISPOR: Intuitive guide selection for CRISPR/Cas9 genome editing experiments and screens. *Nucleic Acids Res.* **46**, W242–W245 (2018).
48. M. Ovesny, P. Křížek, J. Borkovec, Z. Svindrych, G. M. Hagen, ThunderSTORM: A comprehensive ImageJ plug-in for PALM and STORM data analysis and super-resolution imaging. *Bioinformatics* **30**, 2389–2390 (2014).
49. Y. Gao, D. Shonai, M. Trn, J. Zhao, E. J. Soderblom, S. A. Garcia-Moreno, C. A. Gersbach, W. C. Wetsel, G. Dawson, D. Velmeshev, Y. H. Jiang, L. G. Sloofman, J. D. Buxbaum, S. H. Soderling, Proximity analysis of native proteomes reveals phenotypic modifiers in a mouse model of autism and related neurodevelopmental conditions. *Nat. Commun.* **15**, 6801 (2024).

Acknowledgments: Figures 1, 3, and 8 were created using BioRender.com. **Funding:** This work was supported by the National Institutes of Health grant R35 NS122073 (M.N.R.), F31 NS139435 (V.P.), and F31 NS134125 (A.J.M.), the Dr. Miriam and Sheldon G. Adelson Medical Research Foundation (M.N.R.), and the McNair Medical Institute at The Robert and Janice McNair Foundation (Y.G.). **Author contributions:** Conceptualization: W.Z., V.P., and M.N.R. Data curation: W.Z. and V.P. Formal analysis: W.Z., V.P., and Y.G. Funding acquisition: V.P., A.J.M., Y.G., and M.N.R. Investigation: W.Z., V.P., X.D., Y.W., A.J.M., and Y.G. Methodology: W.Z., V.P., X.D., and Y.O. Project administration: M.N.R. Resources: W.Z., Y.G., Y.O., and M.N.R. Supervision: M.N.R. Validation: W.Z., V.P., and X.D. Visualization: W.Z., V.P., A.J.M., Y.G., and M.N.R. Writing—original draft: W.Z., V.P., and M.N.R. Writing—review and editing: W.Z., V.P., Y.W., Y.G., and M.N.R. **Competing interests:** Y.G. has a patent application related to the HiUGE technology (16/968,904). M.N.R. is a paid consultant for Contineum Therapeutics. All other authors declare that they have no competing interests. **Data and materials availability:** All data needed to evaluate the conclusions in the paper are present in the paper and/or the Supplementary Materials. Data are available from Dataverse: https://doi.org/10.7910/DVN/NORKXE.

Submitted 5 December 2024
Accepted 18 April 2025
Published 23 May 2025
10.1126/sciadv.adv1281